

Identification of signaling pathways, matrix-digestion enzymes, and motility components  
controlling *Vibrio cholerae* biofilm dispersal

Andrew A. Bridges<sup>1,2</sup>, Chenyi Fei<sup>1</sup>, Bonnie L. Bassler<sup>1,2\*</sup>

<sup>1</sup>Department of Molecular Biology, Princeton University, Princeton, NJ 08544, USA

<sup>2</sup>The Howard Hughes Medical Institute, Chevy Chase, MD 20815, USA.

\*Corresponding author. Email: [bbassler@princeton.edu](mailto:bbassler@princeton.edu)

Classification: Biological Sciences - Microbiology

Keywords: biofilm dispersal, *Vibrio cholerae*, high-content imaging, signal transduction, matrix digestion, virulence

The authors declare no competing interest.

1 Abstract

2 Bacteria alternate between being free-swimming and existing as members of sessile  
3 multicellular communities called biofilms. The biofilm lifecycle occurs in three stages: cell  
4 attachment, biofilm maturation, and biofilm dispersal. *Vibrio cholerae* biofilms are hyper-infectious  
5 and biofilm formation and dispersal are considered central to disease transmission. While biofilm  
6 formation is well-studied, almost nothing is known about biofilm dispersal. Here, we conduct an  
7 imaging screen for *V. cholerae* mutants that fail to disperse, revealing three classes of dispersal  
8 components: signal transduction proteins, matrix-degradation enzymes, and motility factors.  
9 Signaling proteins dominated the screen and among them, we focused on an uncharacterized  
10 two-component sensory system that we name DbfS/DbfR for Dispersal of Biofilm  
11 Sensor/Regulator. Phospho-DbfR represses biofilm dispersal. DbfS dephosphorylates and  
12 thereby inactivates DbfR, which permits dispersal. Matrix degradation requires two enzymes:  
13 LapG, which cleaves adhesins, and RbmB, which digests matrix polysaccharide. Reorientations  
14 in swimming direction, mediated by CheY3, are necessary for cells to escape from the porous  
15 biofilm matrix. We suggest that these components act sequentially: signaling launches dispersal  
16 by terminating matrix production and triggering matrix digestion and, subsequently, cell motility  
17 permits escape from biofilms. This study lays the groundwork for interventions that modulate *V.*  
18 *cholerae* biofilm dispersal to ameliorate disease.

19 Significance statement

20 The pathogen *Vibrio cholerae* alternates between the free-swimming state and existing in  
21 sessile multicellular communities known as biofilms. Transitioning between these lifestyles is key  
22 for disease transmission. *V. cholerae* biofilm formation is well studied, however, almost nothing  
23 is known about how *V. cholerae* cells disperse from biofilms, precluding understanding of a central  
24 pathogenicity step. Here, we conducted a high-content imaging screen for *V. cholerae* mutants  
25 that failed to disperse. Our screen revealed three classes of components required for dispersal:  
26 signal transduction, matrix degradation, and motility factors. We characterized these components  
27 to reveal the sequence of molecular events that choreograph *V. cholerae* biofilm dispersal. Our  
28 report provides a framework for developing strategies to modulate biofilm dispersal to prevent or  
29 treat disease.

## 30 Main

31 Bacteria transition between existing in the biofilm state, in which cells are members of  
32 surface-associated multicellular collectives, and living as free-swimming, exploratory individuals.  
33 Biofilms consist of cells surrounded by a self-secreted extracellular matrix that protects the  
34 resident cells from threats including predation, antimicrobials, and dislocation due to flow.(1–3)  
35 Biofilms are relevant to human health because beneficial microbiome bacteria exist in biofilms,  
36 and, during disease, because pathogens in biofilms evade host immune defenses, thwart medical  
37 intervention, and exhibit virulence.(4–7) The biofilm lifecycle consists of three stages: cell  
38 attachment, biofilm maturation, and dispersal (Figure 1A).(8) Cells liberated during the dispersal  
39 step can disseminate and found new biofilms.(8) The environmental stimuli and the components  
40 facilitating biofilm attachment and maturation have been defined for many bacterial species.(9) In  
41 contrast, little is known about the biofilm dispersal stage.

42 The model pathogen *Vibrio cholerae* forms biofilms in its aquatic habitat, biofilm cells are  
43 especially virulent in mouse models of cholera disease, and biofilms are thought to be critical for  
44 cholera transmission.(10–14) Studies of *V. cholerae* biofilms have predominantly focused on  
45 matrix overproducing strains that constitutively exist in the biofilm mode and that do not disperse.  
46 This research strategy has propelled understanding of *V. cholerae* biofilm attachment and  
47 maturation, revealing that the second messenger cyclic diguanylate (c-di-GMP) is a master  
48 regulator of biofilm formation, and that expression of vibrio polysaccharide (*vps*) biosynthetic  
49 genes are required.(15–17) The strategy of characterizing constitutive biofilm formers, while  
50 successful for uncovering factors that promote biofilm formation, has necessarily precluded  
51 studies of biofilm dispersal. Here, we employed a microscopy assay that allowed us to monitor  
52 the full wild-type (WT) *V. cholerae* biofilm lifecycle. We combined this assay with high-content  
53 imaging of randomly mutagenized WT *V. cholerae* to identify genes required for biofilm dispersal.  
54 Investigation of the proteins encoded by the genes allowed us to characterize the signaling relays,  
55 matrix-digestion enzymes, and motility components required for biofilm dispersal, a key stage in  
56 the lifecycle of the global pathogen *V. cholerae*.

## 57 **Results**

58 Previously, we developed a brightfield microscopy assay that allows us to monitor the full  
59 WT *V. cholerae* biofilm lifecycle in real time.(18) In our approach, *V. cholerae* cells are inoculated  
60 onto glass coverslips at low cell density and brightfield time-lapse microscopy is used to monitor  
61 biofilm progression. WT biofilms reach peak biomass after 8–9 h of incubation and subsequently  
62 dispersal occurs and is completed by 12–13 h (Figure 1B, C). To identify genes required for biofilm  
63 dispersal, we combined mutagenesis with high-content imaging of the output of this assay.  
64 Specifically, WT *V. cholerae* was mutagenized with Tn5 yielding ~7000 mutants that were arrayed  
65 in 96-well plates. Following overnight growth, the mutants were diluted to low cell density in  
66 minimal medium, a condition that drives initiation of the biofilm lifecycle. Brightfield images of each  
67 well were captured 8 h post-inoculation to assess biofilm maturation and at 13 h to evaluate biofilm  
68 dispersal. Mutants that showed no defects in biofilm maturation as judged by the 8 h images but  
69 displayed significant remaining biofilm biomass at the 13 h timepoint were identified. To verify  
70 phenotypes, candidate mutants were individually reevaluated by time-lapse microscopy. Mutants  
71 that accumulated at the bottom of wells due to aggregation or that failed to attach to surfaces  
72 were excluded from further analysis, eliminating strains harboring insertions in O-antigen and  
73 flagellar genes, respectively. The locations of transposon insertions in the 47 mutants that met  
74 our criteria were defined and corresponded to 10 loci. The new genes from the screen fell into

75 three classes: signal transduction (blue), matrix degradation (green), and motility (red) (Figure  
76 1A, C). In-frame deletions of each gene were constructed, and the biofilm lifecycles of the deletion  
77 mutants were imaged to confirm that the genes are required for biofilm dispersal (Table 1, Video  
78 1). We also identified insertions in genes encoding proteins with known roles in biofilm dispersal  
79 (i.e., RpoS, quorum sensing), which we excluded from further analysis. (18, 19)

Figure 1

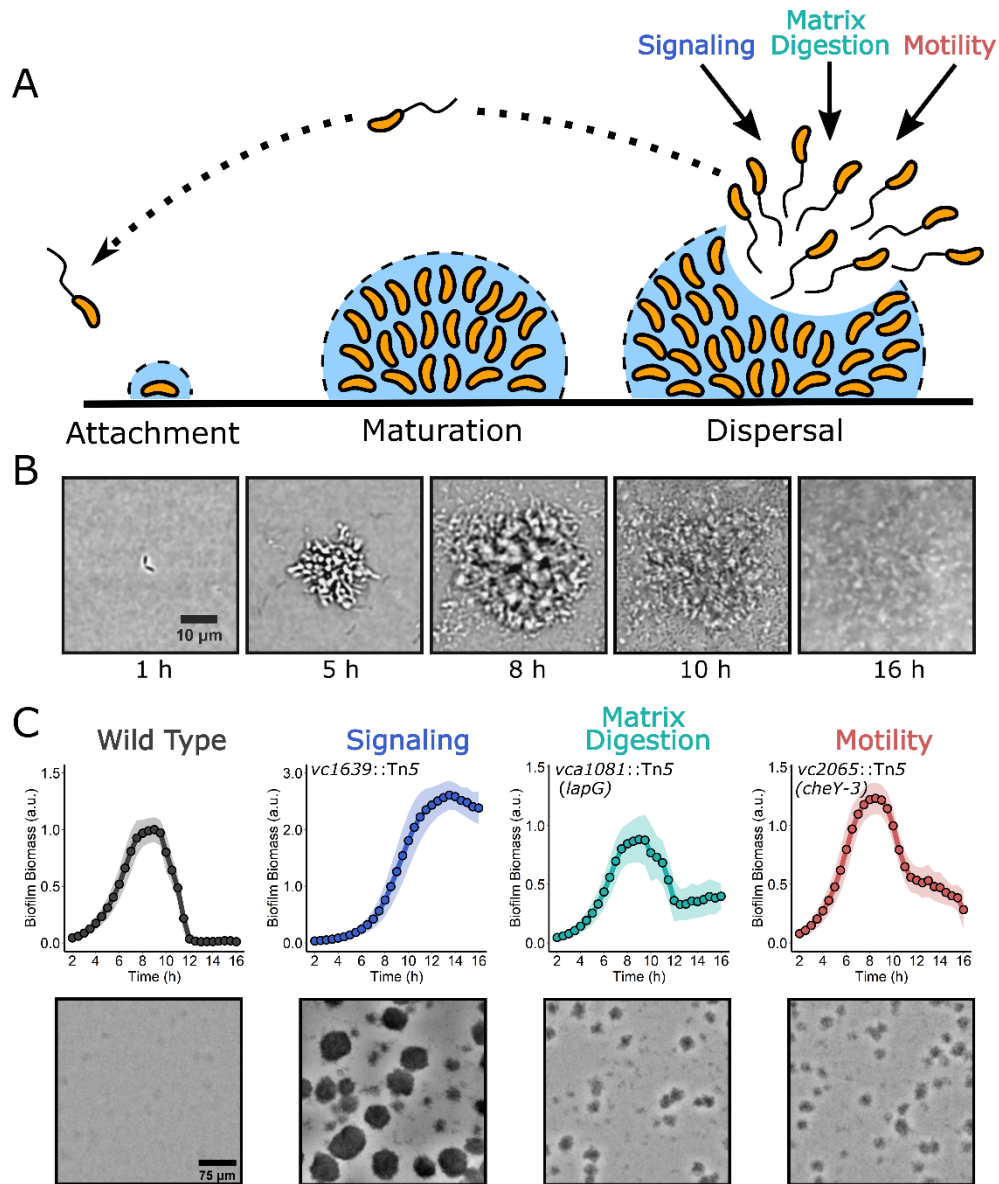


Figure 1. **A high-content imaging screen identifies genes required for *V. cholerae* biofilm dispersal.** (A) Schematic illustrating the *V. cholerae* biofilm lifecycle. See text for details. (B) Brightfield image series over time of the WT *V. cholerae* biofilm lifecycle. (C) Top panels: Quantitation of biofilm biomass over time as measured by time-lapse microscopy for WT and representative transposon insertion mutants from each of the three functional categories identified in the screen. Note differences in y-axes scales. Data are represented as means normalized to the peak biofilm biomass of the WT strain.  $N = 3$  biological and  $N = 3$  technical replicates,  $\pm$  SD (shaded). a.u., arbitrary unit. Bottom panels: Representative brightfield images of biofilms at the final 16 h timepoint for the strains presented in the top panels.

80 Proteins involved in signal transduction dominated the screen (7 of 10 loci) and included the  
 81 ribosome-associated GTPase, BipA, multiple cyclic diguanylate (c-di-GMP) signaling proteins,  
 82 polyamine signaling proteins, and a putative two-component histidine kinase, Vc1639. The signal  
 83 transduction mutants displayed different severities in their biofilm dispersal phenotypes. The  
 84  $\Delta bipA$  displayed a modest defect: ~19% of its biofilm biomass remained at 16 h, the final timepoint  
 85 of our data acquisition, while the WT showed ~6% biomass remaining. By contrast, the  $\Delta vc1639$   
 86 mutant underwent no appreciable dispersal (Table 1). In the category of matrix degradation, two  
 87 enzymes were identified, LapG a periplasmic protease, and RbmB, a putative polysaccharide  
 88 lyase (Table 1). A single motility mutant was identified with an insertion in the gene encoding the  
 89 chemotaxis response regulator *cheY3* (Table 1). Below, we carry out mechanistic studies on  
 90 select mutants from each category to define the functions of the components. Other mutants will  
 91 be characterized in separate reports.

**Table 1:** Genes identified as required for *V. cholerae* biofilm dispersal and phenotypes of deletion mutants.

Gene	Function	Functional Category	Times Hit	Peak Biomass (vs WT)	Peak Time	% Biomass Remaining (16 h)
WT	-	-	-	1.0 ± 0.2	8.7 ± 0.4 h	6 ± 4%
<i>bipA</i> (vc2744)	ribosome-associated GTPase	Signaling	2	1.0 ± 0.2	9.6 ± 0.3 h	19 ± 6%
<i>cdgG</i> (vc0900)	GGDEF domain containing protein	Signaling	1	1.1 ± 0.3	8.4 ± 0.6 h	34 ± 13%
<i>cdgI</i> (vc0658)	c-di-GMP phosphodiesterase	Signaling	1	0.9 ± 0.2	8.7 ± 0.4 h	17 ± 9%
<i>rocS</i> (vc0653)	c-di-GMP phosphodiesterase	Signaling	1	1.3 ± 0.3	10.4 ± 0.6 h	59 ± 13%
<i>mbaA</i> (vc0703)	polyamine sensor, c-di-GMP phosphodiesterase	Signaling	2	0.9 ± 0.2	9.6 ± 0.3 h	27 ± 10%
<i>potD1</i> (vc1424)	polyamine transporter	Signaling	6*	1.6 ± 0.2	11.9 ± 0.9 h	90 ± 12%
<i>dbfS</i> (vc1639)	histidine kinase	Signaling	8	1.8 ± 0.3	14.3 ± 0.9 h	95 ± 8%
<i>lapG</i> (vca1081)	peptidase	Matrix Digestion	3	0.8 ± 0.2	9.4 ± 0.2 h	55 ± 12%
<i>rbmB</i> (vc0929)	polysaccharide lyase	Matrix Digestion	21	0.9 ± 0.2	10 ± 0.4 h	69 ± 12%
<i>cheY3</i> (vc2065)	chemotaxis response regulator	Motility	2*	1.0 ± 0.2	9.1 ± 0.6 h	21 ± 6%

All ± values represent SD

\*Value includes transposon insertions in other genes in this operon

## 92 **A two-component regulatory system controls *V. cholerae* biofilm dispersal**

93 The mutant from our screen that exhibited the most extreme dispersal phenotype had a  
94 transposon in a gene encoding an uncharacterized putative histidine kinase (designated HK),  
95 Vc1639 (Table 1). A screen for factors required for *V. cholerae* colonization of the suckling mouse  
96 intestine repeatedly identified Vc1639, suggesting that this HK is core to the cholera disease.(20)  
97 HKs typically contain periplasmic ligand binding domains and internal catalytic domains that  
98 switch between kinase and phosphatase activities based on ligand detection.(21) HKs transmit  
99 sensory information to cognate response regulators (RR) by altering RR phosphorylation.(22)  
100 RRs, in turn, control gene expression and/or behavior depending on their phosphorylation states.  
101 Deletion of *vc1639* in *V. cholerae* resulted in an 80% increase in peak biofilm biomass relative to  
102 WT and nearly all the biofilm biomass remained at 16 h demonstrating that Vc1639 is essential  
103 for biofilm dispersal (Figure 2A, Table 1). Complementation of the  $\Delta vc1639$  mutant with *vc1639*  
104 inserted onto the chromosome at an ectopic locus restored WT biofilm dispersal (Supplementary  
105 Figure 1A). Consistent with the extreme dispersal phenotype of the  $\Delta vc1639$  mutant, *vpsL-lux*  
106 expression was elevated 10-fold throughout the growth curve in the  $\Delta vc1639$  strain compared to  
107 WT *V. cholerae* (Figure 2B). *vpsL* is the first gene in the major extracellular matrix biosynthetic  
108 operon showing that Vc1639 signaling regulates matrix production. Likewise, *lux* promoter fusions  
109 to the genes encoding the biofilm master regulators *vpsR* and *vpsT* also exhibited increased light  
110 production in the  $\Delta vc1639$  mutant suggesting that VC1639 acts at the top of the cascade to control  
111 global biofilm gene expression (Supplementary Figure 1B, C). *vc1639* is the final gene in a three  
112 gene operon that includes genes encoding a hypothetical protein (Vc1637) and an OmpR family  
113 RR (Vc1638) (Figure 2C). We name Vc1639 DbfS for Dispersal of Biofilm Sensor and we name  
114 Vc1638 DbfR for Dispersal of Biofilm Regulator. Domain prediction suggests that DbfS contains  
115 two transmembrane domains (TM), a periplasmic sensory domain, and a cytoplasmic HAMP  
116 domain that likely transmits ligand-binding-induced conformational changes to regulation of the  
117 C-terminal kinase/phosphatase activity (Figure 2C).

118 To explore the connection between DbfS and DbfR in the control of biofilm dispersal, we  
119 deleted *dbfR*. Commonly, cognate HK and RR null mutants have identical phenotypes. To our  
120 surprise, the  $\Delta dbfR$  mutant had no biofilm dispersal defect and progressed through the biofilm  
121 lifecycle identically to WT (Figure 2D). We considered the possibility that some other RR is the  
122 partner to DbfS. To test this idea, we constructed the  $\Delta dbfS \Delta dbfR$  double mutant. This strain  
123 behaved identically to the  $\Delta dbfR$  strain (Figure 2D), demonstrating that *dbfR* is epistatic to *dbfS*  
124 and thus, DbfR indeed functions downstream of DbfS. Moreover, because RRs are typically active  
125 when phosphorylated, our results suggest that DbfR must be active in the absence of DbfS. Thus,  
126 we reason that phospho-DbfR is the species present in the  $\Delta dbfS$  strain. To verify the hypothesis  
127 that phospho-DbfR is responsible for the dispersal defect in the  $\Delta dbfS$  strain, we constructed a  
128 non-phosphorylatable allele of DbfR (D51V). The *V. cholerae dbfR<sup>D51V</sup>* mutant displayed the WT  
129 biofilm dispersal phenotype in the presence and the absence of DbfS (Figure 2E). DbfR-SNAP  
130 fusions showed that SNAP did not interfere with WT DbfR function and that DbfR protein  
131 abundance was unchanged in the *dbfR<sup>D51V</sup>* strain relative to WT (Supplementary Figure 1D, E).  
132 Thus, phospho-DbfR causes *V. cholerae* cells to remain in the biofilm state in the  $\Delta dbfS$  mutant.  
133 It follows that deletion of *dbfS* causes biofilm dispersal failure due to loss of DbfS phosphatase  
134 activity on DbfR. To test this hypothesis, we assessed *in vivo* DbfR phosphorylation in the  
135 presence and absence of DbfS. Phos-tag gel analysis enabled separation and visualization of  
136 phosphorylated and dephosphorylated DbfR. In the absence of DbfS, DbfR was phosphorylated



**Figure 2**

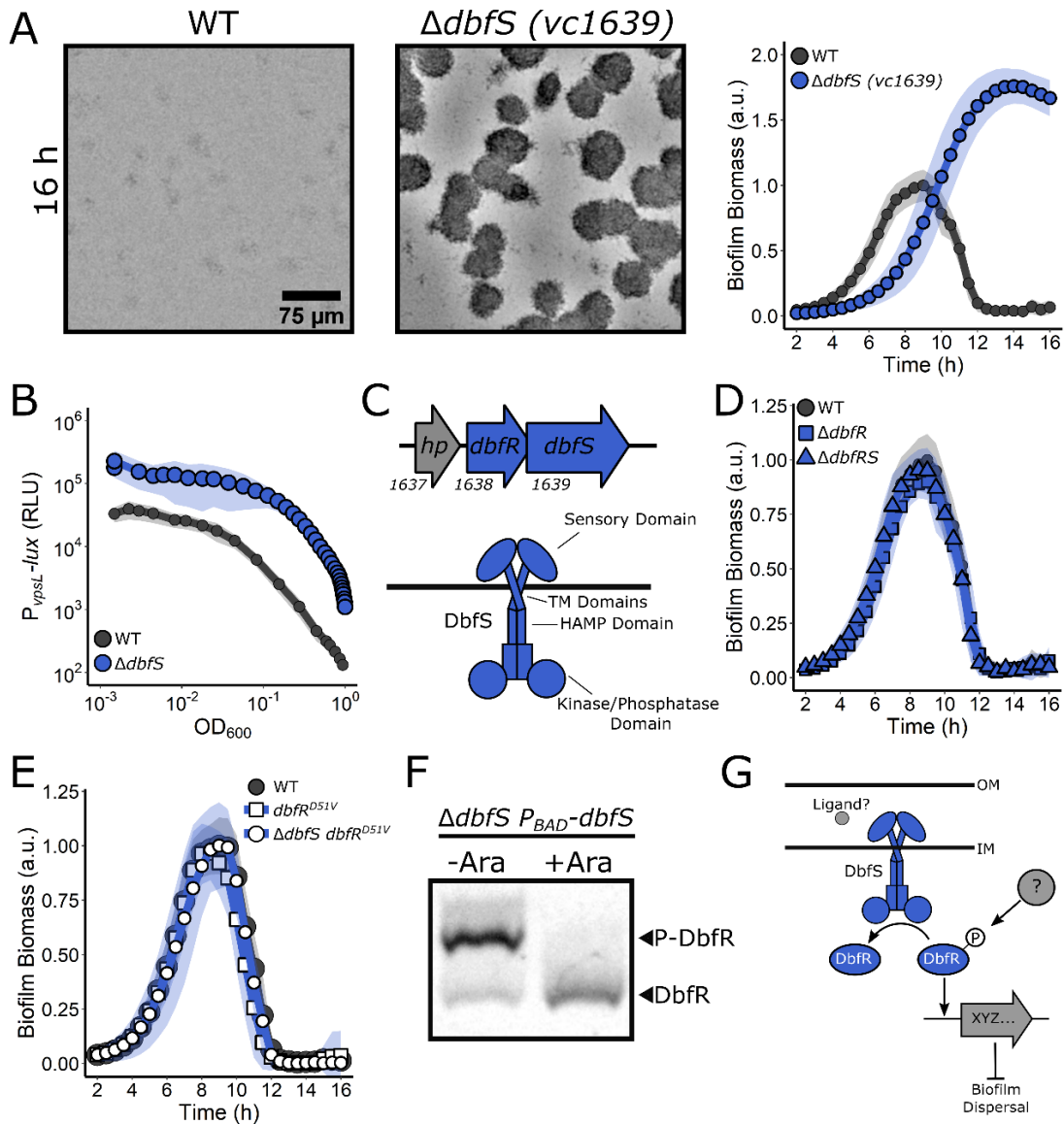


**Figure 2. A two-component system composed of DbfS (HK) and DbfR (RR) controls *V. cholerae* biofilm dispersal.** (A) Representative 16 h images and quantitation of biofilm biomass over time measured by time-lapse microscopy for WT *V. cholerae* and the  $\Delta dbfS$  (i.e.,  $\Delta vc1639$ ) mutant. (B) The corresponding  $P_{vpsL-lux}$  output for strains and growth conditions in A over the growth curve. (C) Top panel: operon structure of the genes encoding the DbfS-DbfR two-component system. Bottom panel: Cartoon of the domain organization of DbfS. TM, transmembrane domain (D) As in A for the  $\Delta dbfR$  (i.e.,  $\Delta vc1638$ ) strain and for the  $\Delta dbfS \Delta dbfR$  double mutant. (E) As in A for the *dbfR*<sup>D51V</sup> and  $\Delta dbfS$  *dbfR*<sup>D51V</sup> strains. (F) Representative Phos-tag gel analysis of DbfR-SNAP in the absence (-arabinose) or presence (+arabinose) of DbfS. Fucose was added to repress DbfR production in the uninduced samples. A phosphorylated protein migrates slower than the same unphosphorylated protein. (G) Proposed model for the DbfS-DbfR phosphorylation cascade regulating biofilm dispersal. OM, outer membrane; IM, inner membrane. In all biofilm measurements,  $N = 3$  biological and  $N = 3$  technical replicates,  $\pm$  SD (shaded). a.u., arbitrary unit. For *vpsL-lux* measurements,  $N = 3$  biological replicates,  $\pm$  SD (shaded). RLU, relative light units. Phos-tag gel result is representative of  $N = 3$  independent biological replicates.

137 and induction of DbfS production caused the phospho-DbfR species to disappear (Figure 2F).  
138 Thus, under our experimental conditions, DbfS functions as a DbfR phosphatase. We infer that  
139 some other unknown kinase must exist and phosphorylate DbfR (Figure 2G). We propose that  
140 phospho-DbfR is active, and it drives expression of matrix biosynthetic genes, and increased  
141 matrix production prevents biofilm dispersal. It is possible that phospho-DbfR also controls other  
142 genes involved in suppressing biofilm dispersal.

143 DbfS is well-conserved in the vibrio genus, for example, in *Vibrio vulnificus* and *Vibrio*  
144 *parahaemolyticus*, DbfS has respectively, 64% and 60% amino acid sequence identity to *V.*  
145 *cholerae* DbfS. In genera closely related to vibrio, i.e., *Allochromobium* and photobacteria, the *dbfS* gene  
146 exists in an identical operon organization and the encoded protein shows high amino acid  
147 sequence identity (~55-65%) to *V. cholerae* DbfS. In many cases, *dbfS* is annotated as *phoQ*,  
148 encoding the well-studied cation-regulated HK from enteric pathogens including *Escherichia coli*  
149 and *Salmonella*. However, BLAST analysis of the DbfS protein sequence against that from *E. coli*  
150 K-12 revealed limited homology to PhoQ, with 32% amino acid sequence identity (E value= $1e^{-41}$ ),  
151 with the lowest region of similarity in the predicted ligand binding domain. We tested whether the  
152 ligands that control PhoQ signal transduction also regulate DbfS-DbfR signaling (Supplementary  
153 Figure 2A-D, Supplemental Discussion). They do not. Thus, DbfS and DbfR are not functionally  
154 equivalent to PhoQ and its cognate RR, PhoP, respectively. Thus, DbfS responds to a yet-to-be  
155 defined stimulus to regulate biofilm dispersal.

#### 156 **Matrix disassembly mediates *V. cholerae* exit from biofilms**

157 The second group of mutants in our screen harbored insertions in the gene encoding the  
158 calcium-dependent periplasmic protease LapG that degrades outer-membrane spanning  
159 adhesive proteins and in the gene specifying the extracellular polysaccharide lyase RbmB that  
160 degrades the VPS component of the biofilm matrix.(23, 24) The  $\Delta lapG$  strain exhibited slightly  
161 lower peak biofilm biomass compared to WT, with a short delay in the onset of dispersal, and  
162 ~55% of its biomass remained at 16 h (Figure 3A, Table 1). The  $\Delta lapG$  and the WT strains had  
163 similar *vpsL-lux* expression patterns (Figure 3B) consistent with LapG playing no role in  
164 repression of matrix production, but rather functioning downstream in matrix degradation. The  
165 LapG mechanism is known: When c-di-GMP concentrations are high, the FrhA and CraA  
166 adhesins are localized to the outer membrane where they facilitate attachments that are important  
167 for biofilm formation (Figure 3C).(25, 26) Under this condition, LapG is sequestered and  
168 inactivated by the inner membrane c-di-GMP sensing protein LapD.(25) When c-di-GMP levels  
169 fall, LapD releases LapG, and LapG cleaves FrhA and CraA facilitating cell detachment from  
170 biofilms.(25) Our results are consistent with this mechanism; in the absence of LapG, FrhA and  
171 CraA remain intact, and *V. cholerae* cells cannot properly exit the biofilm state. To verify that the  
172 established c-di-GMP-dependent regulatory mechanism controls LapG activity in our assay, we  
173 deleted *lapD* (Figure 3C). Indeed, in the  $\Delta lapD$  strain, biofilm dispersal occurred prematurely  
174 indicating that, without LapD, LapG is not sequestered, and unchecked LapG activity promotes  
175 premature adhesin degradation, and, as a consequence, early biofilm disassembly (Figure 3D).  
176 The  $\Delta lapD \Delta lapG$  double mutant had the same dispersal phenotype as the  $\Delta lapG$  single mutant  
177 confirming that LapG functions downstream of LapD (Figure 3D). Lastly, in a reciprocal  
178 arrangement, overexpression of *lapG* from an ectopic locus caused peak biofilm formation to  
179 decrease by ~65% (Supplementary Figure 3A) suggesting that enhanced LapG-mediated  
180 cleavage of adhesins prematurely released cells from the biofilm. Thus, the conserved Lap



181 pathway, which responds to changes in c-di-GMP levels, facilitates biofilm dispersal in *V.*  
 182 *cholerae*.

**Figure 3**

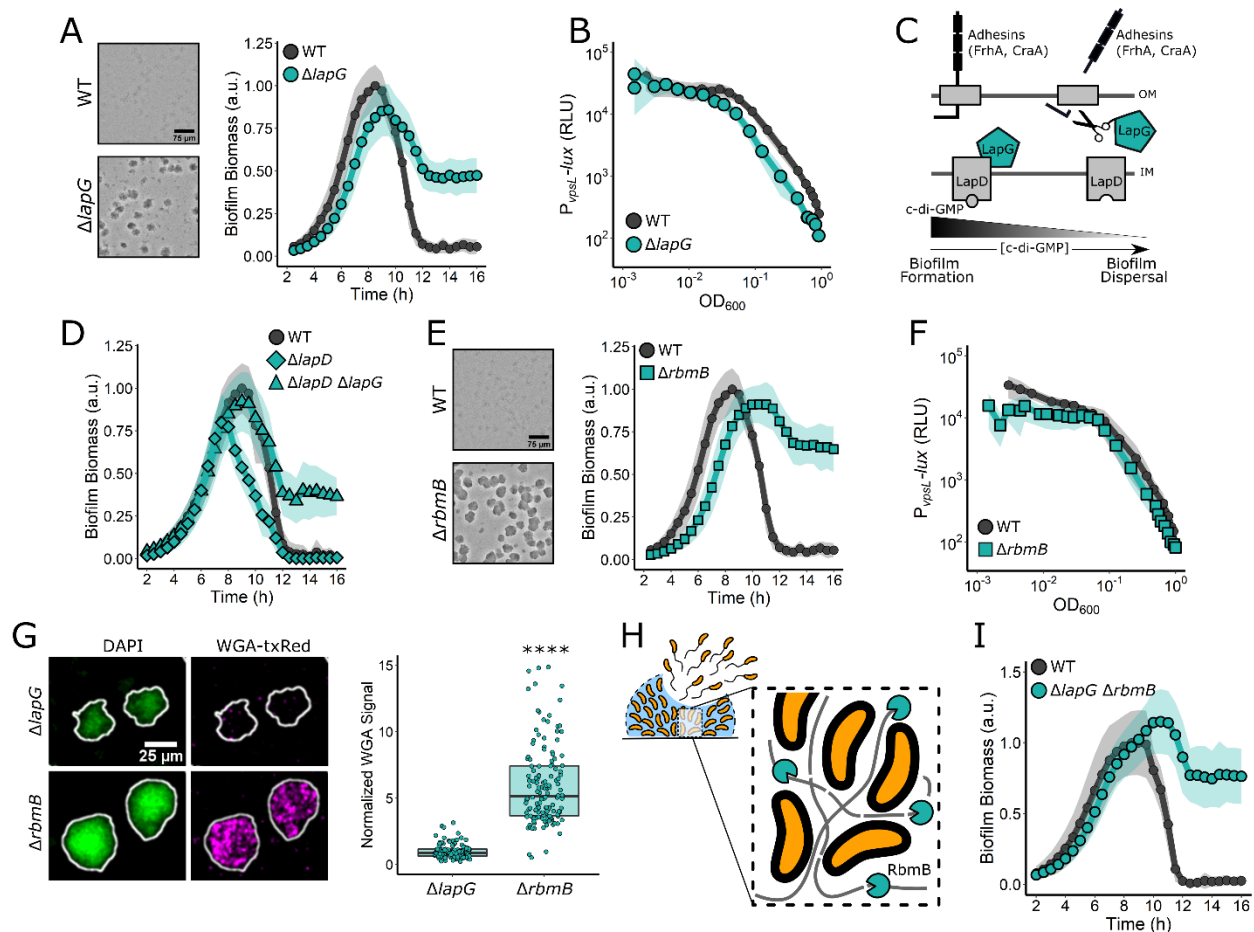


**Figure 3. Matrix-digesting enzymes mediate *V. cholerae* biofilm dispersal.** (A) Representative 16 h images and quantitation of biofilm biomass over time measured by time-lapse microscopy for WT *V. cholerae* and the  $\Delta lapG$  mutant. (B) The corresponding  $P_{vpsL-lux}$  output for strains and growth conditions in A over the growth curve. (C) Schematic representing the LapG mechanism. (D) As in A for the WT, the  $\Delta lapD$  single mutant, and the  $\Delta lapD \Delta lapG$  double mutant. (E) As in A for the WT and the  $\Delta rbmB$  mutant. (F) As in B for WT *V. cholerae* and the  $\Delta rbmB$  mutant. (G) Representative images and quantitation of WGA-txRed signal in  $\Delta lapG$  and  $\Delta rbmB$  biofilms 16 h post-inoculation. To account for differences in biomass, the WGA-txRed signal was divided by the 4', 6-diamidino-2-phenylindole (DAPI) signal in each biofilm. Values were normalized to the mean signal for the  $\Delta lapG$  strain. >100 individual biofilms were quantified for each strain. An unpaired t-test was performed for statistical analysis, with \*\*\*\* denoting  $p < 0.0001$ . (H) Proposed model for the role of RbmB in biofilm dispersal. Gray lines represent the polysaccharide matrix. (I) As in A for the WT and the  $\Delta lapG \Delta rbmB$  double mutant. In all cases,  $N = 3$  biological and  $N = 3$  technical replicates,  $\pm$  SD (shaded). a.u., arbitrary unit. For  $vpsL-lux$  measurements,  $N = 3$  biological replicates,  $\pm$  SD (shaded). RLU, relative light units. OM, outer membrane; IM, inner membrane.

183           Regarding the RbmB polysaccharide lyase, the  $\Delta rbmB$  strain formed biofilms to roughly  
184 the same peak biomass as WT, however, it exhibited a 2 h delay in dispersal onset and most of  
185 its biomass (~70%) remained at 16 h (Figure 3E, Table 1). The level of *vpsL-lux* expression in the  
186  $\Delta rbmB$  mutant was similar to the WT, showing that the RbmB dispersal function does not concern  
187 production of VPS (Figure 3F). Complementation with inducible *rbmB* expressed from an ectopic  
188 locus in the  $\Delta rbmB$  strain caused a ~40% reduction in peak biofilm formation, confirming that  
189 RbmB negatively regulates biofilm formation, however the complemented strain retained a  
190 modest biofilm dispersal defect, suggesting that the timing or level of *rbmB* expression is critical  
191 for WT biofilm disassembly (Supplementary Figure 3B). To verify that the  $\Delta rbmB$  dispersal defect  
192 stems from the lack of *vps* degradation, we grew  $\Delta rbmB$  biofilms for 16 h (i.e., post WT  
193 biofilm dispersal completion), and subsequently fixed and stained the non-dispersed biofilms with  
194 wheat germ agglutinin conjugated to Texas Red (WGA-txRed), which binds to N-  
195 acetylglucosamine sugars in the VPS matrix.(27) We used the  $\Delta lapG$  mutant as our control since  
196 its biofilm dispersal phenotype should not involve changes in VPS. On average, the  $\Delta rbmB$  mutant  
197 exhibited ~6x more WGA-txRed signal than the  $\Delta lapG$  mutant (Figure 3G). Collectively, our results  
198 show that the non-dispersed  $\Delta lapG$  biofilms contain little VPS, consistent with possession of  
199 functional RbmB, while non-dispersed  $\Delta rbmB$  biofilms contain excess VPS due to the lack of  
200 RbmB-mediated polysaccharide digestion. Thus, we suggest that RbmB-directed VPS  
201 disassembly is critical for proper biofilm disassembly (Figure 3H). Our results show that LapG and  
202 RbmB function in different pathways to drive biofilm disassembly. To examine their combined  
203 effects, we constructed the  $\Delta lapG \Delta rbmB$  double mutant and measured its biofilm lifecycle (Figure  
204 3I). The  $\Delta lapG \Delta rbmB$  double mutant mimicked the single  $\Delta rbmB$  mutant (Figure 3E) in its biofilm  
205 dispersal defect. Thus, the  $\Delta lapG$  and  $\Delta rbmB$  defects are not additive. Presumably, the severe  
206 dispersal defect displayed by the  $\Delta rbmB$  single mutant, which cannot digest matrix  
207 polysaccharides, is not made more extreme by additional impairment of matrix protein  
208 degradation, suggesting that cells are already maximally trapped by the undigested  
209 polysaccharides.

210           Extracellular DNA (eDNA) is a component of the *V. cholerae* biofilm matrix and two  
211 DNases secreted by *V. cholerae*, Dns and Xds, digest eDNA.(28) Although we did not identify  
212 *dns* and *xds* in our screen, we nonetheless investigated whether they contributed to biofilm  
213 dispersal. Neither the  $\Delta dns$  and the  $\Delta xds$  single mutants, nor the  $\Delta dns \Delta xds$  double mutant  
214 displayed a biofilm dispersal defect in our assay (Supplementary Figure 3C), suggesting that  
215 eDNA digestion is not required for dispersal. In a similar vein, we did not identify genes encoding  
216 the eight *V. cholerae* extracellular proteases that could degrade matrix proteins. Consistent with  
217 this finding, measurement of the phenotypes of mutants deleted for each extracellular protease  
218 gene showed that none exhibited a dispersal defect. Thus, no single extracellular protease is  
219 required for biofilm dispersal (Supplementary Figure 3D). It remains possible that proteases  
220 contribute to biofilm dispersal by functioning redundantly. Together, our results indicate that two  
221 enzymes, LapG and RbmB, are the primary matrix degrading components that enable biofilm  
222 dispersal.

### 223 **Reorientations in swimming direction are required for biofilm dispersal.**

224           The final category of genes identified in our screen are involved in cell motility. As noted  
225 above, non-motile mutants were excluded from analysis because they are known to be impaired  
226 in surface attachment. Nonetheless, we identified a mutant containing a transposon insertion in  
227 *cheY3* as defective for biofilm dispersal. *cheY3* is one of the five *V. cholerae* *cheY* genes

228 specifying chemotaxis RR proteins.(29) Notably, *cheY3* is the only *V. cholerae cheY* homolog  
229 required for chemotaxis.(29) The  $\Delta cheY3$  mutant exhibited similar peak biofilm timing and  
230 biomass as WT *V. cholerae*, however, ~21% biomass remained at 16 h (Figure 4A, Table 1).  
231 Complementation via introduction of *cheY3* at an ectopic locus restored biofilm dispersal in the  
232 mutant (Supplementary Figure 4A). Expression of *vpsL-lux* in the  $\Delta cheY3$  mutant was identical to  
233 the WT indicating that the dispersal phenotype was not due to elevated matrix production (Figure  
234 4B).

235 The *V. cholerae* default motor rotation direction is counterclockwise (CCW), which fosters  
236 smooth, straight swimming.(30) Transition to clockwise (CW) motor rotation causes reorientations  
237 in swimming direction.(30) Phospho-CheY3 binds to the flagellar motor switch complex to mediate  
238 the change from CCW to CW rotation. Thus, the  $\Delta cheY3$  mutant is non-chemotactic and the cells  
239 are locked in the CCW, straight swimming mode (Figure 4C). We reasoned that the  $\Delta cheY3$   
240 mutant dispersal defect could stem from an inability to chemotact or from an inability to reorient  
241 swimming direction. To distinguish between these possibilities, we examined biofilm dispersal in  
242 a *V. cholerae* mutant carrying a *cheY3* allele, *cheY3*<sup>D16K, Y109W</sup> (henceforth, *cheY3*<sup>\*</sup>) that locks the  
243 motor into CW rotation and so also disrupts chemotaxis. *cheY3*<sup>\*</sup> cells undergo frequent  
244 reorientations and are unable to swim in smooth straight runs (Figure 4C).(29, 31) The *cheY3*<sup>\*</sup>  
245 strain had WT biofilm dispersal capability. Thus, being chemotactic is not required for *V. cholerae*  
246 to exit biofilms (Figure 4A).

247 We reasoned that analysis of the unique motility characteristics of our strains could reveal  
248 the underlying causes of the  $\Delta cheY3$  biofilm dispersal defect. We measured the turning  
249 frequencies and swimming velocities of the WT,  $\Delta cheY3$ , and *cheY3*<sup>\*</sup> *V. cholerae* strains.  
250 Consistent with previous reports, these three mutants exhibited notable differences: on average,  
251 the WT turned once every 3 s, the  $\Delta cheY3$  mutant turned less than once every 40 s, and the  
252 *cheY3*<sup>\*</sup> strain turned once every 0.5 s (Figure 4C and D).(29, 31) The *cheY3*<sup>\*</sup> strain displayed  
253 slightly lower average swimming velocity than the WT and  $\Delta cheY3$  strains, due to its high turning  
254 frequency as turning necessarily involves a decrease in velocity (Figure 4E).(32) Together, these  
255 results suggest that the low turning frequency of the  $\Delta cheY3$  mutant is responsible for the biofilm  
256 dispersal defect. We propose that if cells do not frequently change their direction of motion, they  
257 become trapped by the biofilm matrix mesh which compromises their ability to escape (Figure  
258 4F). Indeed, in other bacteria, straight-swimming mutants are deficient in traversing fluid-filled  
259 porous media compared to WT organisms that can reorient.(33) Together, these results indicate  
260 that chemotaxis itself is not required for biofilm dispersal, but, rather, that the chemotaxis  
261 machinery facilitates random reorientation events that allow *V. cholerae* cells to navigate a porous  
262 biofilm matrix. The same non-chemotactic mutants used here exhibit stark differences in  
263 competition experiments in animal models of cholera infection, showing that their differences in  
264 motility and, possibly, their differences in biofilm dispersal capabilities, are pertinent to  
265 colonization.(31)

266 Finally, we determined whether the ability to locomote was required for biofilm dispersal  
267 or, by contrast, if non-motile cells could escape the digested matrix via Brownian motion. As  
268 mentioned above, we could not simply study dispersal of non-flagellated and non-motile mutants  
269 because of their confounding surface attachment defects and feedback on biofilm regulatory  
270 components.(34, 35) To circumvent this problem, we employed phenamil, an inhibitor of the Na<sup>+</sup>-  
271 driven *V. cholerae* flagellar motor, which, as expected, dramatically reduced planktonic cell  
272 motility (Supplementary Figure 4B).(36) To assess the role of swimming motility in biofilm

**Figure 4**

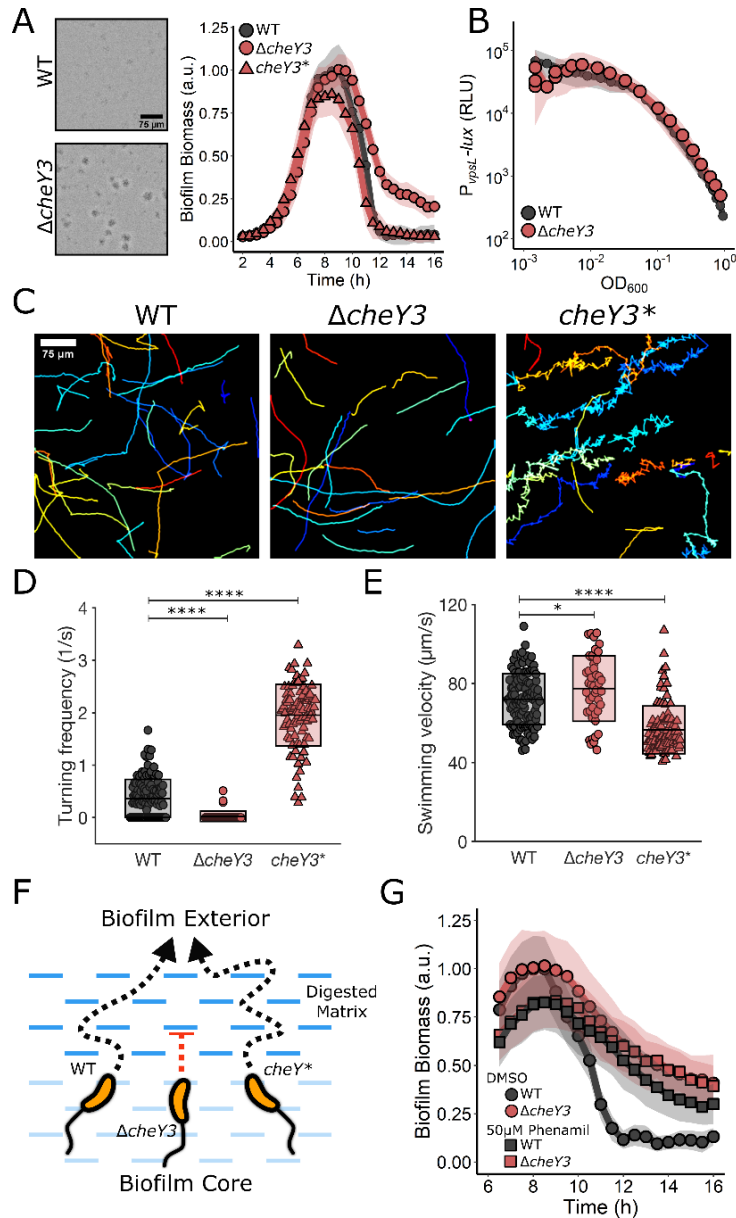


**Figure 4. Reorientations in swimming direction are required for *V. cholerae* biofilm dispersal.** (A) Representative 16 h images and quantitation of biofilm biomass over time measured by time-lapse microscopy for WT *V. cholerae*, the  $\Delta cheY3$  mutant, and the  $cheY3^{D16K, Y109W}$  ( $cheY3^*$ ) mutant. (B) The corresponding  $P_{vpsL-lux}$  output for WT and the  $\Delta cheY3$  strain over the growth curve. (C) Representative, randomly colored, single-cell locomotion trajectories for the strains in A. (D) Turning frequencies of the strains in A. (E) Measured swimming velocities of the strains in A. (F) Proposed model for the role of motility and reorientation in biofilm dispersal. (G) Quantitation of biofilm biomass over time for WT and the  $\Delta cheY3$  mutant following treatment with DMSO or the motility inhibitor, phenamil supplied at 5 h post-inoculation. For biofilm biomass assays,  $N = 3$  biological and  $N = 3$  technical replicates,  $\pm$  SD (shaded). a.u., arbitrary unit. For  $vpsL-lux$  measurements,  $N = 3$  biological replicates,  $\pm$  SD (shaded). RLU, relative light units. For motility measurements, 45-125 individual cells of each strain were tracked. In panels D and E, unpaired t-tests were performed for statistical analysis, with P values denoted as \* $P < 0.05$ ; \*\* $P < 0.01$ ; \*\*\*  $P < 0.001$ ; \*\*\*\* $P < 0.0001$ ; n.s.,  $P > 0.05$ .

273 dispersal, we first allowed WT *V. cholerae* cells to undergo biofilm formation for 5 h, at which point  
274 we perfused DMSO or phenamil into the incubation chamber (Figure 4G). Following phenamil  
275 treatment, the WT strain displayed a dispersal defect nearly identical to that of the  $\Delta cheY3$  mutant.  
276 Additionally, phenamil treatment of the  $\Delta cheY3$  mutant did not further impair its biofilm dispersal.  
277 Together, these results demonstrate that swimming motility is crucial for *V. cholerae* biofilm  
278 dispersal and an inability to reorient is as detrimental to dispersal as a complete lack of flagellar  
279 motility.

## 280 Discussion

281 In this study, we developed a high-content imaging screen that allowed us to identify  
282 components required for *V. cholerae* biofilm dispersal. We categorized the identified components  
283 into three classes: signal transduction, matrix disassembly, and cell motility. We propose that the  
284 three functional categories represent the chronological steps required for the disassembly of a  
285 biofilm: First, the stimuli that activate dispersal must accumulate. Subsequently, the gene  
286 expression pattern established by detection of these stimuli must repress biofilm matrix production  
287 and activate production of enzymes required to digest the biofilm matrix. Finally, cells must  
288 escape through the partially digested, porous matrix which requires changes in the direction of  
289 movement. Together, these steps ensure that when environmental conditions are appropriate, *V.*  
290 *cholerae* cells can exit the sessile lifestyle and disseminate to new terrain that is ripe for biofilm  
291 formation or, alternatively, during disease, to a new host. One can now imagine targeting the  
292 functions identified in this work for small-molecule disruption of the *V. cholerae* biofilm lifecycle,  
293 possibly guiding the development of treatments to reduce the duration of *V. cholerae* infection or  
294 to prevent transmission.

## 295 Materials and Methods

### 296 **Bacterial Strains and Reagents**

297 The *V. cholerae* parent strain used in this study was WT O1 El Tor biotype C6706str2. Antibiotics  
298 were used at the following concentrations: polymyxin B, 50  $\mu\text{g}/\text{mL}$ ; kanamycin, 50  $\mu\text{g}/\text{mL}$ ;  
299 spectinomycin, 200  $\mu\text{g}/\text{mL}$ ; and chloramphenicol, 1  $\mu\text{g}/\text{mL}$ . Strains were propagated in lysogeny  
300 broth (LB) supplemented with 1.5% agar or in liquid LB with shaking at 30°C. All strains used in  
301 this work are reported in Supplementary Table 1. Unless otherwise stated, exogenous  
302 compounds were added from the onset of biofilm initiation. The antimicrobial peptide C18G  
303 (VWR) was added at 5  $\mu\text{g}/\text{mL}$ . Phenamil (Sigma) was prepared in DMSO and added 5 h post  
304 biofilm inoculation to a final concentration of 50  $\mu\text{M}$ . L-arabinose (Sigma) was prepared in water  
305 and added at 0.2%.

### 306 **DNA Manipulation and Strain Construction**

307 To produce linear DNA fragments for natural transformations, splicing overlap extension  
308 PCR was performed using iProof polymerase (Bio-Rad, Hercules, CA, USA) to combine DNA  
309 pieces. Primers and gene fragments used in this study are reported in Supplementary Table 2. In  
310 all cases, ~3 kb of upstream and downstream flanking regions of homology were generated by  
311 PCR from *V. cholerae* genomic DNA and were included to ensure high chromosomal integration  
312 frequency. DNA fragments that were not native to *V. cholerae* were synthesized as g-blocks (IDT,  
313 Coralville, IA, USA).



314 All *V. cholerae* strains generated in this work were constructed by replacing genomic DNA  
315 with DNA introduced by natural transformation as previously described.(18, 37) The neutral  
316 *vc1807* locus was used as the site of introduction of the gene encoding the antibiotic resistance  
317 cassette in the natural co-transformation procedure. The *vc1807* locus was also used as the site  
318 for introduction of genes under study in chromosomal ectopic expression analyses.(37) PCR and  
319 Sanger sequencing were used to verify correct integration events. Genomic DNA from  
320 recombinant strains was used for future co-transformations and as templates for PCR to generate  
321 DNA fragments, when necessary. Deletions were constructed in frame and eliminated the entire  
322 coding sequences. The exceptions were *mbaA*, *dbfS*, and *dbfR*, which each overlap with another  
323 gene in their operons. In these cases, portions of the genes were deleted ensuring that adjacent  
324 genes were not perturbed. For *tagA*, the first 103 base pairs, including the nucleotides specifying  
325 the start codon, were deleted. All strains constructed in this study were verified by sequencing at  
326 Genewiz.

### 327 **Microscopy and Mutant Screening**

328 The biofilm lifecycle was measured using time-lapse microscopy as described  
329 previously.(18) All plots were generated using ggplot2 in R. To generate the library of *V. cholerae*  
330 insertion mutants for the dispersal screen, the WT parent strain was mutagenized with Tn5 as  
331 previously described.(38) Mutants were selected by growth overnight on LB plates containing  
332 polymyxin B and kanamycin. The next day, mutant colonies were arrayed into 96-well plates  
333 containing 200  $\mu$ L of LB medium supplemented with polymyxin B and kanamycin using an  
334 automated colony-picking robot (Molecular Devices). The arrayed cultures were grown in a plate-  
335 shaking incubator at 30° C covered with breathe-easy membranes to minimize evaporation. After  
336 16 h of growth, the arrayed cultures were diluted 1:200,000 into 96-well plates containing M9  
337 medium supplemented with glucose and casamino acids. Diluted cultures were incubated  
338 statically at 30° C for 8 h (to achieve peak biofilm biomass), at which point, images of each well  
339 were captured on a Nikon Ti-E inverted microscope using transmitted-light bright-field illumination,  
340 a 10 $\times$  Plan Fluor (NA 0.3) objective lens, and an Andor iXon 897 EMCCD camera. Automated  
341 image acquisition was performed using NIS-Elements software v5.11.02 and the NIS-Elements  
342 Jobs Module to acquire images at four positions within each well to account for heterogeneity  
343 within samples. To maintain the focal plane between wells, the Nikon Perfect Focus System was  
344 used. After performing microscopy at the 8 h timepoint, 96-well plates were returned to the  
345 incubator. To assess biofilm dispersal, a second set of images of the same samples was acquired  
346 at 13 h post inoculation. Mutants that displayed biofilm growth at the 8 h timepoint but failed to  
347 disperse by the 13 h timepoint were subcultured, grown overnight, and subsequently re-imaged  
348 using the time-lapse approach described above to assess their biofilm lifecycles in real-time.  
349 Mutants that exhibited biofilm dispersal defects after this reassessment step were analyzed for  
350 the locations of transposon insertions using arbitrary PCR.(39)

### 351 ***lux* Transcription Assays**

352 Three colonies of each strain to be analyzed were individually grown overnight in 200  $\mu$ L  
353 LB with shaking at 30°C in a 96-well plate covered with a breathe-easy membrane. The following  
354 morning, the cultures were diluted 1:5,000 into fresh M9 medium supplemented with glucose and  
355 casamino acids. The plates were placed in a BioTek Synergy Neo2 Multi-Mode reader (BioTek,  
356 Winooski, VT, USA) under static growth conditions at 30°C. Both OD<sub>600</sub> and bioluminescence  
357 from the *lux* fusions were simultaneously measured at 15 min time intervals. Results were

358 exported to R, and light values were divided by OD<sub>600</sub> to produce relative light units (RLUs).  
359 Results from replicates were averaged and plotted using ggplot2 in R.

### 360 **VPS Quantitation**

361 To assess VPS levels in non-dispersed biofilms using WGA-txRED, biofilms were grown for 16 h  
362 and subsequently washed 3 times with 1× phosphate buffered saline (PBS), and fixed for 10 min  
363 with 3.7% formaldehyde in 1× PBS. After fixation, samples were washed 5 times with 1× PBS and  
364 subsequently incubated with a solution containing 1 µg/mL WGA-txRED (ThermoFisher  
365 Scientific), 1 µg/mL 4', 6-diamidino-2-phenylindole (DAPI), and 1% bovine serum albumin in 1×  
366 PBS for 1 h with shaking at 30° C in the dark. After incubation, samples were washed 5 more  
367 times with 1× PBS before imaging. Confocal microscopy was performed on a Leica DMI8 SP-8  
368 point scanning confocal microscope (Leica, Wetzlar, Germany) with the pinhole set to 1.0 airy  
369 unit. The light source for DAPI was a 405 laser and the light source used to excite WGA-txRED  
370 was a tunable white-light laser (Leica; model #WLL2; excitation window = 470–670 nm) set to 595  
371 nm. Biofilms were imaged using a 10× air objective (Leica, HC PL FLUOTAR; NA: 0.30).  
372 Sequential frame scanning was performed to minimize spectral bleed-through in images. Emitted  
373 light was detected using GaAsP spectral detectors (Leica, HyD SP), and timed gate detection  
374 was employed to minimize the background signal. Image analyses were performed in FIJI  
375 software (Version 1.52p). Biofilms were segmented in the DAPI channel using an intensity  
376 threshold and the intensities of each channel were measured. The same threshold was applied  
377 to all images. WGA-txRED signal was divided by DAPI signal to achieve the normalized WGA  
378 signal.

### 379 **Motility Assay**

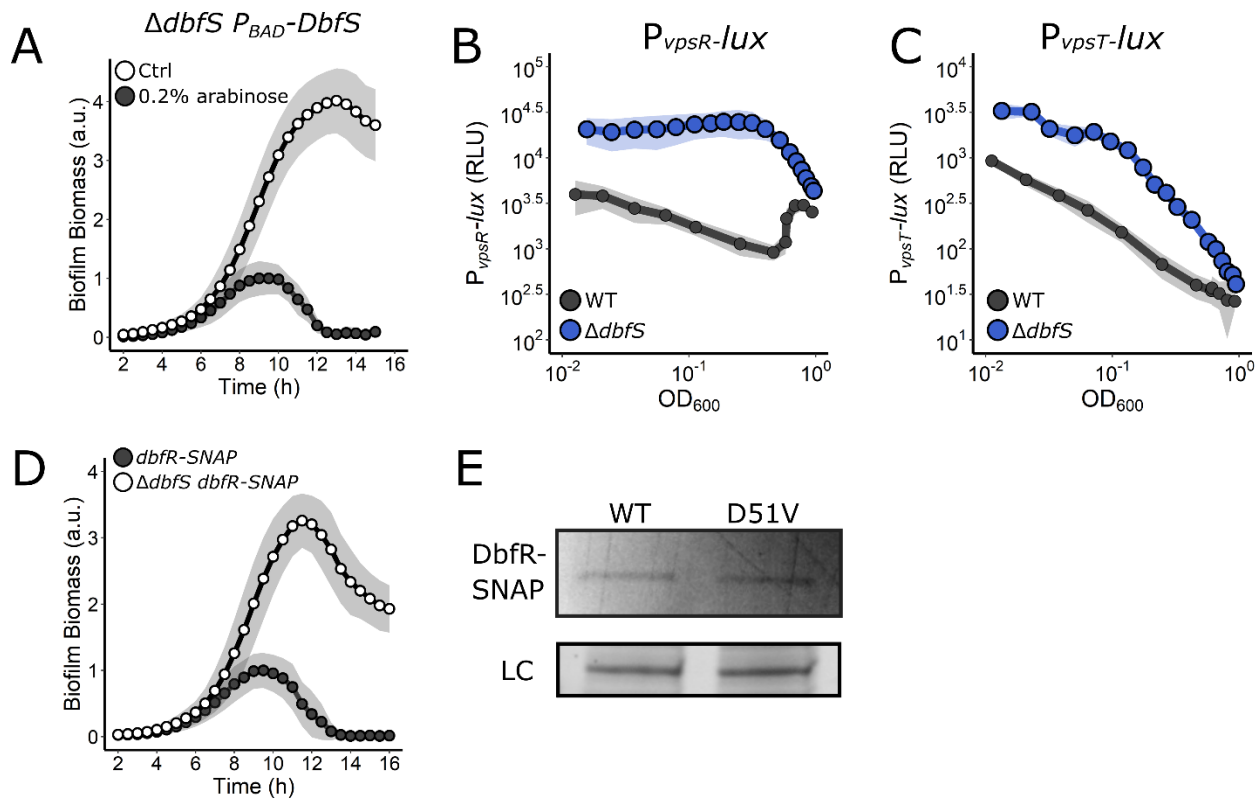
380 To prevent biofilm formation during measurements of swimming velocities and turning  
381 frequencies for the WT,  $\Delta cheY3$ , and  $cheY3^*$  strains, *vpsL* was deleted. Each strain was grown  
382 for 16 h in LB medium and the following day, cells were diluted to OD<sub>600</sub> = 0.001 in M9 medium  
383 supplemented with glucose and casamino acids. Subsequently, diluted cultures were dispensed  
384 in 200 µL aliquots into glass-coverslip bottomed 96-well plates (MatTek, Ashland, MA, USA). After  
385 a period of 1 h, during which time cells were allowed to adhere to the coverslips, wells were  
386 washed 8 times with fresh medium to remove unattached cells. The plates were incubated at 25°  
387 C for 3 h, and imaging was performed using the brightfield setup described above for the biofilm  
388 dispersal screen. In this case, the frame interval was 50 msec and imaging was conducted at a  
389 distance of ~100 µm into the sample. Images were smoothed, background corrected, and  
390 imported into the TrackMate (v.5.2.0) plugin in FIJI. Cells were detected with a Laplacian of  
391 Gaussian (LoG) detector and were subsequently tracked using the simple Linear Assignment  
392 Problem (LAP) approach. To exclude non-motile cells from our analyses in Figure 4C-E objects  
393 with velocities under 40 µm/sec were eliminated. Analyses and plotting of swimming velocities  
394 and turning frequencies were performed in MATLAB (The Mathworks, Inc.). Local curvatures for  
395 single-cell locomotion trajectories were calculated as described.(40) Curvature of less than 0.3  
396 µm<sup>-1</sup> was used to identify the turning events. MSD was calculated as described previously.(41)

### 397 **Phos-tag Gel Analysis**

398 To monitor DbfR and phospho-DbfR via SDS-PAGE, the endogenous *dfbR* gene was  
399 replaced with *dbfR-SNAP* in the  $\Delta dbfS$  strain, and *P<sub>BAD</sub>-dbfS* was introduced at the ectopic locus,

400 *vc1807*. To assess DbfR-SNAP phosphorylation in the absence and presence of DbfS, overnight  
401 cultures of the strain were diluted 1:1000 and subsequently grown for 4 h at 30° C with shaking  
402 to an OD<sub>600</sub> ~ 0.6. To each culture, 1 μM SNAP-Cell TMR Star (New England Biolabs) was added  
403 to label the SNAP tag, and the culture was subsequently divided into two tubes. To one tube,  
404 0.2% D-fucose was added, and to the other, 0.2% L-arabinose was added to repress and induce  
405 DbfS production, respectively. The cultures were returned to 30° C with shaking. After 1 h, the  
406 cells were collected by centrifugation for 1 min at 13,000 rpm. Lysis and solubilization were carried  
407 out as rapidly as possible. Briefly, cells were chemically lysed by resuspension to OD<sub>600</sub> = 1.0 in  
408 40 μL Bug Buster (Novagen) for 5 min at 25° C with intermittent vortex. The cell lysate was  
409 solubilized at 25° C in 1.5× SDS-PAGE buffer for 5 min also with intermittent vortex. Samples  
410 were immediately loaded onto a cold 7.5% SuperSep™ Phos-tag™ (50 μM/L) gel (FUJIFILM  
411 Wako Pure Chemical, 198-17981). Electrophoresis was carried out at 100 V at 4° C until the  
412 loading buffer exited the gel. Gel images were captured on an ImageQuant LAS 4000 imager (GE  
413 Healthcare) using a Cy3 filter set.

Supplementary Figure 1



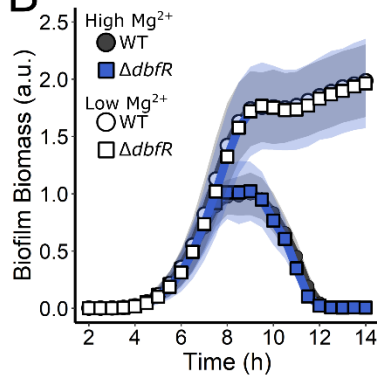
Supplementary Figure 1. **Complementation, functional tagging, and mutagenesis of the DbfS-DbfR two-component system.** (A) Quantitation of biofilm biomass over time measured by time-lapse microscopy for the  $\Delta dbfS$   $P_{BAD}$ - $dbfS$  strain following addition of water (Ctrl) or 0.2% arabinose. (B)  $P_{vpsR}$ - $lux$  and (C)  $P_{vpsT}$ - $lux$  output for WT and the  $\Delta dbfS$  strain over the growth curve. (D) As in A for SNAP-tagged DbfR in the WT and  $\Delta dbfS$  strains. (E) Top panel: representative in-gel SDS-PAGE fluorescence following electrophoresis of *V. cholerae* cell lysates containing WT DbfS-SNAP or DbfS<sup>D51V</sup>-SNAP that had been incubated with SNAP-Cell TMR Star. Bottom panel: Coomassie stained loading control (LC). For all biofilm measurements,  $N = 3$  biological and  $N = 3$  technical replicates,  $\pm$  SD (shaded). a.u., arbitrary unit. For  $lux$  measurements,  $N = 3$  biological replicates,  $\pm$  SD (shaded). RLU, relative light units.

## Supplementary Figure 2

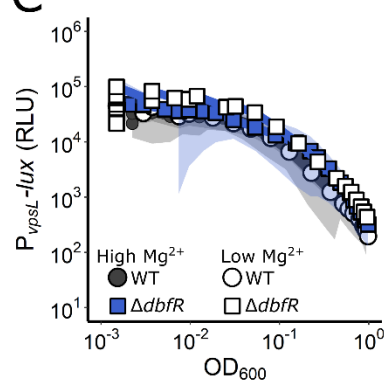
### A



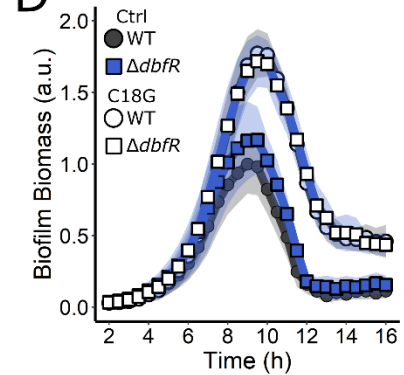
### B



### C



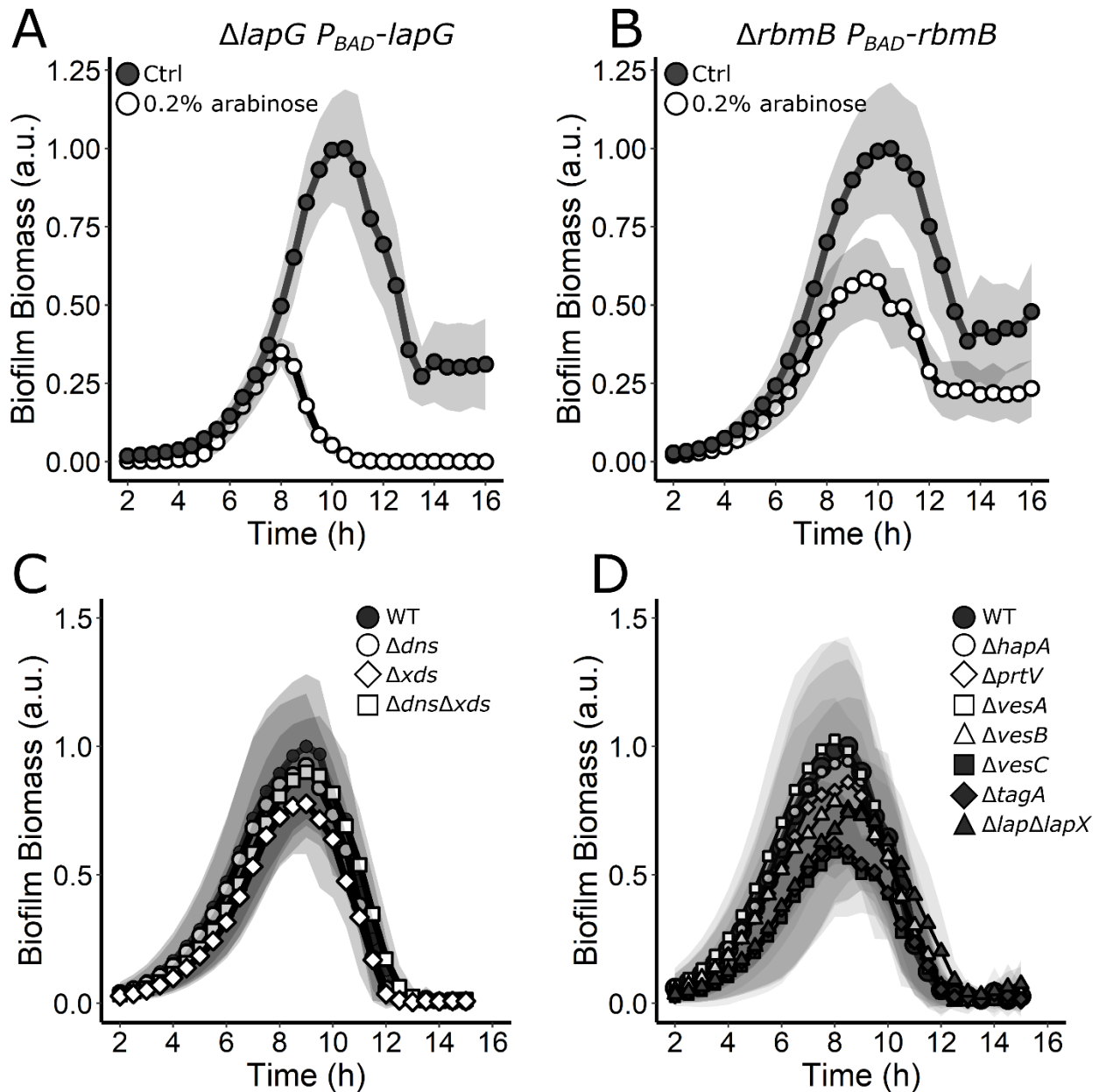
### D



**Supplementary Figure 2. DbfS is not functionally equivalent to PhoQ.** (A) Alignment of the sensory domains of PhoQ from *E. coli*, *S. enterica*, and *P. aeruginosa* against that of *V. cholerae* DbfS. Black boxes indicate residues involved in  $Mg^{2+}$  binding in PhoQ. (B) Quantitation of biofilm biomass over time measured by time-lapse microscopy in high magnesium (10 mM) and limiting magnesium (10  $\mu$ M) conditions for WT *V. cholerae* and the  $\Delta dbfR$  strain. (C) The corresponding  $P_{vpsL-lux}$  outputs for strains and growth conditions in B over the growth curve. (D) As in B except following the addition of water or 5  $\mu$ g/mL C18G. In all cases,  $N = 3$  biological and  $N = 3$  technical replicates,  $\pm$  SD (shaded). a.u., arbitrary unit. For  $vpsL-lux$  measurements,  $N = 3$  biological replicates,  $\pm$  SD (shaded). RLU, relative light units.

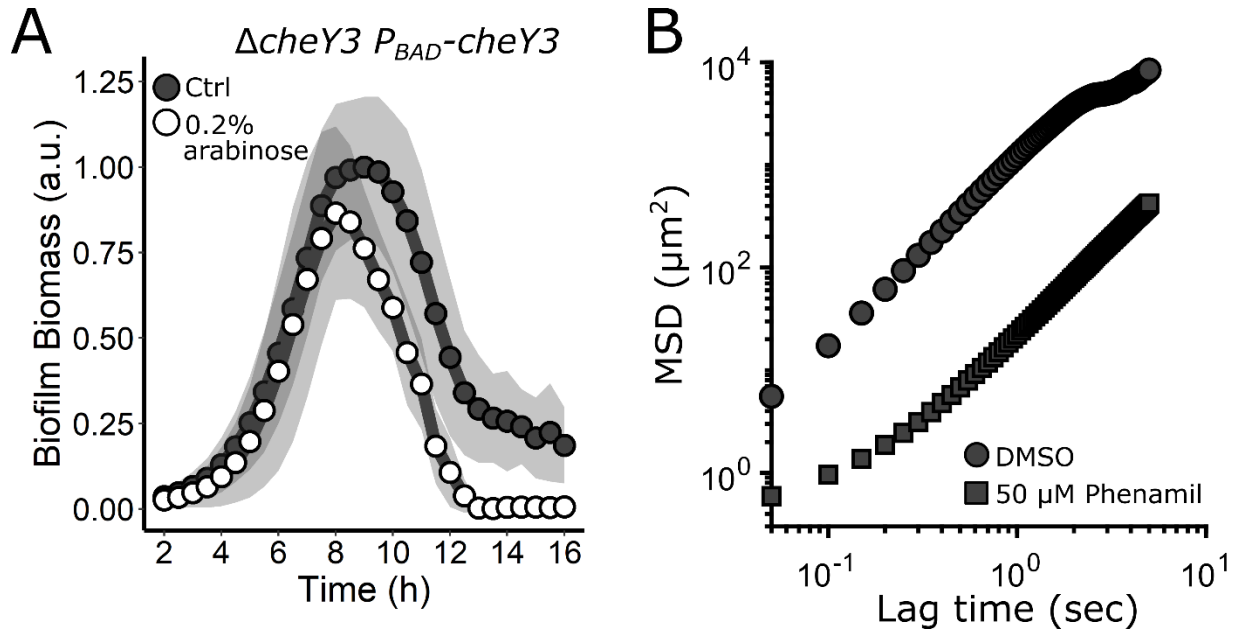


Supplementary Figure 3



Supplementary Figure 3. **Introduction of *lapG* and *rbmB* complements the  $\Delta lapG$  and  $\Delta rbmB$  biofilm defects, respectively, and assessment of the roles of extracellular DNases and secreted proteases in *V. cholerae* biofilm dispersal.** (A) Quantitation of biofilm biomass over time measured by time-lapse microscopy for the  $\Delta lapG P_{BAD-lapG}$  strain following addition of water (Ctrl) or 0.2% arabinose. (B) As in A, but for the  $\Delta rbmB P_{BAD-rbmB}$  strain. (C) Quantitation of biofilm biomass over time measured by time-lapse microscopy for WT *V. cholerae* and mutants lacking the designated DNases. (D) Quantitation of biofilm biomass over time measured by time-lapse microscopy for WT *V. cholerae* and mutants lacking the designated proteases. In all cases,  $N = 3$  biological and  $N = 3$  technical replicates,  $\pm$  SD (shaded). a.u., arbitrary unit.

Supplementary Figure 4



Supplementary Figure 4. **Complementation of the  $\Delta cheY3$  mutant and phenamil inhibition of *V. cholerae* motility.** (A) Quantitation of biofilm biomass over time measured by time-lapse microscopy for the  $\Delta cheY3 P_{BAD}-cheY3$  strain following addition of water (Ctrl) or 0.2% arabinose. In all cases,  $N = 3$  biological and  $N = 3$  technical replicates,  $\pm$  SD (shaded). a.u., arbitrary unit. (B) Mean squared displacement (MSD) of cell trajectories versus lag time for WT *V. cholerae* treated with DMSO solvent or 50  $\mu M$  phenamil.

## Supplemental Discussion

### *DfbS is not equivalent to PhoQ*

In *E. coli*, low  $Mg^{2+}$  and cationic peptides activate PhoQ kinase activity.(42) Sequence alignment of the DfbS sensory domain with that from PhoQ of *E. coli*, *Salmonella enterica*, and *Pseudomonas aeruginosa* revealed that DfbS lacks all of the key residues involved in  $Mg^{2+}$  binding (Supplementary Figure 2A).(43) To test if  $Mg^{2+}$  alters DfbS activity, we measured the *V. cholerae* biofilm lifecycle in response to low  $Mg^{2+}$  conditions in WT *V. cholerae* and in the  $\Delta dbfR$  mutant. If, analogous to PhoQ, DfbS kinase activity is activated by low  $Mg^{2+}$ , when  $Mg^{2+}$  is limiting, WT *V. cholerae* should exhibit an altered biofilm dispersal phenotype while the  $\Delta dbfR$  mutant would be impervious to  $Mg^{2+}$  changes.(42) Supplementary Figure 2B shows that  $Mg^{2+}$  limitation does indeed inhibit *V. cholerae* biofilm dispersal, however, inhibition occurs in *both* the WT and the  $\Delta dbfR$  strains.  $Mg^{2+}$  limitation did not alter *vpsL-lux* expression in either strain (Supplementary Figure 2C). Thus,  $Mg^{2+}$  does not control DfbS activity. We obtained the same results following exogenous addition of the cationic peptide C18G (Supplementary Figure 2D). Together, these results demonstrate that DfbS does not respond to the ligands that control PhoQ activity.

## **Acknowledgements**

We thank members of the Bassler group and Prof. Ned Wingreen for thoughtful discussions. We particularly thank Dr. Matthew Jemielita for help with the secreted protease mutants used in this study. This work was supported by the Howard Hughes Medical Institute, NIH Grant 5R37GM065859, National Science Foundation Grant MCB-1713731, and a Max Planck-Alexander von Humboldt research award to BLB. AAB is a Howard Hughes Medical Institute Fellow of the Damon Runyon Cancer Research Foundation, DRG-2302-17. The content is solely the responsibility of the authors and does not necessarily represent the official views of the National Institutes of Health. The funders had no role in study design, data collection and analysis, decision to publish, or preparation of the manuscript.

## Supplementary Table 1

Strains used in this study.

Strain Number	Genotype	Plasmid	Antibiotic Resistance	Parent
BB_Vc_0090	WT O1 EI Tor biotype C6706str2	-	Sm	-
AB_Vc_761	$\Delta vlc1807::Cm^R$ (Referred to as WT)	-	Sm, Cm	BB_Vc_0090
AB_Vc_705	$\Delta cheY \Delta vlc1807::Cm^R$	-	Sm, Cm	BB_Vc_0090
AB_Vc_708	$\Delta bipA \Delta vlc1807::Cm^R$	-	Sm, Cm	BB_Vc_0090
AB_Vc_839	$\Delta mbaA \Delta vlc1807::Cm^R$	-	Sm, Cm	BB_Vc_0090
AB_Vc_711	$\Delta potD1 \Delta vlc1807::Cm^R$	-	Sm, Cm	BB_Vc_0090
AB_Vc_757	$\Delta lapG \Delta vlc1807::Cm^R$	-	Sm, Cm	BB_Vc_0090
AB_Vc_758	$\Delta rocS \Delta vlc1807::Cm^R$	-	Sm, Cm	BB_Vc_0090
AB_Vc_775	$\Delta dbfS \Delta vlc1807::Cm^R$	-	Sm, Cm	BB_Vc_0090
AB_Vc_777	$\Delta cdgI \Delta vlc1807::Cm^R$	-	Sm, Cm	BB_Vc_0090
AB_Vc_778	$\Delta cdgG \Delta vlc1807::Cm^R$	-	Sm, Cm	BB_Vc_0090
AB_Vc_485	$\Delta rbmB \Delta vlc1807::Kan^R$	-	Sm, Kan	BB_Vc_0090
AB_Vc_801	$\Delta vlc1807::Kan^R$	pEVS143- $P_{vpsL}$ - $lux::Cm^R$	Sm, Cm, Kan	AB_Vc_479
AB_Vc_825	$\Delta cheY \Delta vlc1807::Kan^R$	pEVS143- $P_{vpsL}$ - $lux::Cm^R$	Sm, Cm, Kan	AB_Vc_705
AB_Vc_829	$\Delta lapG \Delta vlc1807::Kan^R$	pEVS143- $P_{vpsL}$ - $lux::Cm^R$	Sm, Cm, Kan	AB_Vc_757
AB_Vc_802	$\Delta rbmB \Delta vlc1807::Kan^R$	pEVS143- $P_{vpsL}$ - $lux::Cm^R$	Sm, Cm, Kan	AB_Vc_485
AB_Vc_815	$\Delta dbfS \Delta vlc1807::Kan^R$	pEVS143- $P_{vpsL}$ - $lux::Cm^R$	Sm, Cm, Kan	AB_Vc_775
AB_Vc_936	WT	pBBR1- $P_{vpsR}$ - $lux::Cm^R$	Sm, Cm	BB_Vc_0090
AB_Vc_938	WT	pBBR1- $P_{vpsT}$ - $lux::Cm^R$	Sm, Cm	BB_Vc_0090
AB_Vc_942	$\Delta dbfS \Delta vlc1807::Kan^R$	pBBR1- $P_{vpsR}$ - $lux::Cm^R$	Sm, Cm, Kan	AB_Vc_815
AB_Vc_944	$\Delta dbfS \Delta vlc1807::Kan^R$	pBBR1- $P_{vpsT}$ - $lux::Cm^R$	Sm, Cm, Kan	AB_Vc_815
AB_Vc_773	$\Delta dbfR \Delta vlc1807::Cm^R$	-	Sm, Cm	BB_Vc_0090
AB_Vc_701	$\Delta dbfRS \Delta vlc1807::Cm^R$	-	Sm, Cm	BB_Vc_0090
AB_Vc_788	$dbfR^{D51V} \Delta vlc1807::Cm^R$	-	Sm, Cm	BB_Vc_0090
AB_Vc_891	$dbfR^{D51V} \Delta dbfS \Delta vlc1807::Kan^R$	-	Sm, Kan	BB_Vc_0090
AB_Vc_863	$dbfR$ -SNAP $\Delta dbfS \Delta vlc1807::P_{BAD}$ - $dbfS::Spec^R$	-	Sm, Spec	BB_Vc_0090
AB_Vc_865	$\Delta dbfS \Delta vlc1807::P_{BAD}$ - $dbfS::Spec^R$	-	Sm, Spec	BB_Vc_0090
AB_Vc_879	$dbfR$ -SNAP $\Delta vlc1807::Kan^R$	-	Sm, Kan	BB_Vc_0090
AB_Vc_881	$dbfR^{D51V}$ -SNAP $\Delta vlc1807::Kan^R$	-	Sm, Kan	BB_Vc_0090
AB_Vc_859	$\Delta lapG \Delta vlc1807::P_{BAD}$ - $lapG::Spec^R$	-	Sm, Spec	AB_Vc_757
AB_Vc_898	$\Delta lapD \Delta vlc1807::Kan^R$	-	Sm, Kan	BB_Vc_0090
AB_Vc_900	$\Delta lapD \Delta lapG \Delta vlc1807::Kan^R$	-	Sm, Kan	BB_Vc_0090
AB_Vc_948	$\Delta lapG \Delta rbmB \Delta vlc1807::Kan^R$	-	Sm, Kan	AB_Vc_182
AB_Vc_862	$\Delta rbmB \Delta vlc1807::P_{BAD}$ - $rbmB::Spec^R$	-	Sm, Spec	AB_Vc_485
BB_Vc_0252	$\Delta dns$	-	Sm	BB_Vc_0090
BB_Vc_0253	$\Delta xds$	-	Sm	BB_Vc_0090
BB_Vc_0254	$\Delta dns \Delta xds$	-	Sm	BB_Vc_0090



MJ_552	$\Delta hapA \Delta vc1807::Kan^R$	-	Sm, Kan	BB_Vc_0090
MJ_553	$\Delta prtV \Delta vc1807::Kan^R$	-	Sm, Kan	BB_Vc_0090
MJ_554	$\Delta vesA \Delta vc1807::Kan^R$	-	Sm, Kan	BB_Vc_0090
MJ_555	$\Delta vesB \Delta vc1807::Kan^R$	-	Sm, Kan	BB_Vc_0090
MJ_562	$\Delta vesC \Delta vc1807::Kan^R$	-	Sm, Kan	BB_Vc_0090
MJ_561	$\Delta lap \Delta lapX lacZ::Ptac-mKO \Delta vc1807::Kan^R$	-	Sm, Kan	BB_Vc_0090
AB_Vc_792	$\Delta tagA \Delta vc1807::Cm^R$	-	Sm, Cm	BB_Vc_0090
AB_Vc_857	$\Delta cheY \Delta vc1807::P_{BAD-cheY3}::Spec^R$	-	Sm, Spec	AB_Vc_705
AB_Vc_715	$cheY^{D16K, Y109W} \Delta vc1807::Kan^R$	-	Sm, Kan	BB_Vc_0090
AB_Vc_732	$\Delta vpsL \Delta vc1807::Ptac-mScarlett::Spec^R$	-	Sm, Spec	BB_Vc_0090
AB_Vc_735	$\Delta cheY \Delta vpsL \Delta vc1807::Ptac-mScarlett::Spec^R$	-	Sm, Spec	AB_Vc_705
AB_Vc_745	$cheY^{D16K, Y109W} \Delta vpsL \Delta vc1807::Ptac-mScarlett::Spec^R$	-	Sm, Spec	AB_Vc_715

## Supplementary Table 2

DNA oligonucleotides and gene fragments used in this study.

Oligo #	Name	Purpose	Direction	5' to 3' Sequence
551	<i>cheY_3000up</i>	Cloning at <i>cheY3</i> locus	F	CAAGCGTTACAACCTCGCAGCCTAG
552	<i>cheY_3000down</i>	Cloning at <i>cheY3</i> locus	R	CACAACCAGACCTACGCGCTGAC
553	<i>cheY_100up</i>	Cloning at <i>cheY3</i> locus	F	GGTGAGGTACTTGGAGTTAGTGAATCTC
554	<i>cheY_100down</i>	Cloning at <i>cheY3</i> locus	R	CACTGAAGCGCTCATCAATCTGAAAG
555	<i>cheY_B</i>	<i>cheY3</i> deletion	R	GAGCACCTTTTGCCGAGCAAAGCCTGAGTTTGAGATCAG TGATATTTAGTCATTCC
556	<i>cheY_C</i>	<i>cheY3</i> deletion	F	GGAATGACTAAATATCACTGATCTCAAACCTCAGGCTTTTGCT GCGGCAAAGGTGCTC
561	<i>cheY_2700up</i>	Cloning at <i>cheY3</i> locus	F	GATGACCGTGTGAGTTTGAATCGAG
562	<i>cheY_2700down</i>	Cloning at <i>cheY3</i> locus	R	CTTCGGTGTAACCAGTTTTGTAAGTAGAAC
563	<i>cheY_up_R</i>	Cloning at <i>cheY3</i> locus	R	GAGTTTGAGATCAGTGATATTTAGTCATTCCGAGTCC
564	<i>cheY_down_R</i>	Cloning at <i>cheY3</i> locus	R	GGCTTTTGCTGCGGCAAAGGTGCTCTATTCC
566	<i>cheY_D16K_Y109W</i>	Gblock for introduction of <i>cheY3</i> point mutation	F	GTTAAGTCTTGGACTCGGAATGACTAAATATCACTGATCTC AAACTCAGTGGAGGCAATTTTGAATAAAAAATGAAGATCCT TATTGTTGATAAGTTTTCAACAATGCGCGGAATCGTTAAAAA CCTACTTCGAGATCTGGGGTTCAATAACACGCAGGAAGCGG ACGATGGCCTAACGGCATTGCCTATGCTCAAGAAAGGTGAT TTGACTTTGTAGTCACAGACTGGAATATGCCCGGTATGCAA GGTATTGACTTGCTTAAAAATATCCGTGCCGACGAAGAAGCTG AAGCACCTGCCTGTACTAATGATCACAGCAGAAGCCAAACG TGAGCAAATCATCGAAGCCGCTCAAGCAGGCGTGAATGGTT GGATCGTAAAACCATTTACCGCTGCTACGCTTAAAGAAAAAT TAGACAAAATTTTGAGCGTTTATAAGGCTTTTGCTGCGGCA AAAGGTGCTCTATTACACGCGCAAAAG
545	<i>bipA_3000up</i>	Cloning at <i>bipA</i> locus	F	GCTGCGTGAGCAGTTGTAATCGAG
546	<i>bipA_3000down</i>	Cloning at <i>bipA</i> locus	R	CAACGCTTTGTAGTTCTGGGATTAGCATATA
547	<i>bipA_100up</i>	Cloning at <i>bipA</i> locus	F	GTCGACGATTTACGCGCAGACATC
548	<i>bipA_100down</i>	Cloning at <i>bipA</i> locus	R	GAGGTATTTCTGGATAGGTGGCATAGC
549	<i>bipA_B</i>	<i>bipA</i> deletion	R	GATGACTTATCTTACCAAACGAAAAGTCAGTGACGGGGTTTG CTTCACTTTTTCATTGAGGCTG
550	<i>bipA_C</i>	<i>bipA</i> deletion	F	CAGCCTCAATGAAAAAGTGAAGCAAACCCCGTCACTGACTT TCGTTTGGTAAGATAAGTCATC
567	<i>bipA_2700up</i>	Cloning at <i>bipA</i> locus	R	CAGTGACTCGTCCAAAATGAGCACTG
568	<i>bipA_2700down</i>	Cloning at <i>bipA</i> locus	R	GATCTAAATCGCCACTGATCCCATCAAG
571	<i>mbaA_3000up</i>	Cloning at <i>mbaA</i> locus	F	GCGCGCTAATCTGAACTCAACCCATAAG
572	<i>mbaA_2700up</i>	Cloning at <i>mbaA</i> locus	F	CGTTAGCATTCCACGCGGTGAGTTAG
711	<i>mbaA_KO2_B</i>	<i>mbaA</i> deletion	R	GGAGGCATGAAGCCATGGGGAGATCTCGCTATGTTTAGCT TCATATTGGTAAGTCACACTG
712	<i>mbaA_KO2_C</i>	<i>mbaA</i> deletion	F	CAGTGTGACTTACCAATATGAAGCTAAACCATAGCGAGATCT CCCCATGGCTTCATGCCTCC
575	<i>mbaA_2700down</i>	Cloning at <i>mbaA</i> locus	R	GATCTCATGACGCGCCTGACGGTATTTAAG
576	<i>mbaA_3000down</i>	Cloning at <i>mbaA</i> locus	R	CATCGTTGCGGATAGTGGAAATTCAATAAAATG

577	<i>mbaA_100up</i>	Cloning at <i>mbaA</i> locus	F	GAAACCTGACATTGCCGAATCAATGC
578	<i>mbaA_100down</i>	Cloning at <i>mbaA</i> locus	R	CCTGCTTCCAATCCGACATAATACTCTGC
539	<i>potD1_3000up</i>	Cloning at <i>potD1</i> locus	F	CTGGAATCCGGTATGTGTGTGATGGTTAG
540	<i>potD1_3000down</i>	Cloning at <i>potD1</i> locus	R	AGAGCGACTAGGTGTTATTGAACTTGGG
541	<i>potD1_100up</i>	Cloning at <i>potD1</i> locus	F	CTAAGAAAAGCATCAAATAGGCAGCCATTG
542	<i>potD1_100down</i>	Cloning at <i>potD1</i> locus	R	GATCTGGAAGAGATTAAGGCGCTCTC
543	<i>potD1_B</i>	<i>potD1</i> deletion	R	GGTGGCTTTTTAATGGGAGATAAAAGGCTACGTTCCCATAGT GTATAGAAAGAACC
544	<i>potD1_C</i>	<i>potD1</i> deletion	F	GGTTCTTTCTATACACTATGGGAACGTAGCCTTTTATCTCCC ATTA AAAAGCCACC
569	<i>potD1_2700up</i>	Cloning at <i>potD1</i> locus	F	CTGATGATTATTGGTACGAGTTTTCTGACTCGTG
570	<i>potD1_2700down</i>	Cloning at <i>potD1</i> locus	R	CGATAATCCAAATCAAATCGAGGTGCAGG
602	<i>lapG_3000up</i>	Cloning at <i>lapG</i> locus	F	CAAACAATTACCCGGTTATTGGGGATG
603	<i>lapG_2700up</i>	Cloning at <i>lapG</i> locus	F	GCATTCCGTCAAAGTGCTCGATATTCATC
604	<i>lapG_100up</i>	Cloning at <i>lapG</i> locus	F	GATCATTCCGGGAATGACCGCTTC
605	<i>lapG_B</i>	Cloning at <i>lapG</i> locus	R	CGACTAGTTGTTTGTATAGCGTCATAGTGCAGGGCGGGCTA TTCCCTCAGCGCATTGCTTTG
606	<i>lapG_C</i>	<i>lapG</i> deletion	F	CAAAGCAATGCGCTGAGGGAATAGCCCGCCCTGCACTATGA CGCTATACAAACA ACTAGTCG
607	<i>lapG_100down</i>	<i>lapG</i> deletion	R	GTGTTGTTGACTTCAGAGCGTTGTTG
608	<i>lapG_2700down</i>	Cloning at <i>lapG</i> locus	R	GTCCAGCCATTAACCAGATCAACAC
609	<i>lapG_3000down</i>	Cloning at <i>lapG</i> locus	R	CAGCGGTA CTGGAATTGTCCTTGC
774	<i>lapD_3000up</i>	Cloning at <i>lapD</i> locus	F	CGCGAATACAAGAAGCGATCATGCAG
775	<i>lapD_2700up</i>	Cloning at <i>lapD</i> locus	F	GCAA ACTTCTGCTTAAGCTCAAGATACTTGC
776	<i>lapD_100up</i>	Cloning at <i>lapD</i> locus	F	CAATTGGCTGGGGACTCTTCGAGAC
777	<i>lapD_B</i>	<i>lapD</i> deletion	R	GTATCTTGCATGCCTCTGACCTTGGAGTGCCTACTCATCATA GCTAAC
778	<i>lapD_C</i>	<i>lapD</i> deletion	F	GTTAGCTATGATGAGTAGGCACTCCAAGGTCAGAGGCATGC AAGATAC
779	<i>lapD_100down</i>	Cloning at <i>lapD</i> locus	R	GTAAGCCGTTGATCAGTGCTTCAGGAG
780	<i>lapD_2700down</i>	Cloning at <i>lapD</i> locus	R	CTAACTACGCGCAGTATGTTGAGTTACAAGCG
781	<i>lapD_3000down</i>	Cloning at <i>lapD</i> locus	R	CGTTCAAGCACAAAGGCGATA TAGACG
784	<i>lapDG_B</i>	<i>lapDG</i> deletion	R	GTATCTTGCATGCCTCTGACCTTGGAGGGCGGGCTATTCCC TCAGCGCATTG
785	<i>lapDG_C</i>	<i>lapDG</i> deletion	F	CAATGCGCTGAGGGAATAGCCCGCCCTCCAAGGTCAGAGG CATGCAAGATAC
610	<i>rocS_3000up</i>	Cloning at <i>rocS</i> locus	F	CAACTCGAGCTTTTCTACCAACCTCAG
611	<i>rocS_2700up</i>	Cloning at <i>rocS</i> locus	F	GCATTTTACCGCCCCATTTTCGC
612	<i>rocS_100up</i>	Cloning at <i>rocS</i> locus	F	CTTCAGGCCAAGATCCTTTTCTACTGTG
613	<i>rocS_B</i>	<i>rocS</i> deletion	R	GGTTTCCACCAATCAGAGTAAAATTAACCCCTTAAAATACTA CCA ACTGTCCGTGCGCGACGACG
614	<i>rocS_C</i>	<i>rocS</i> deletion	F	CGTCGTCGCGCACGGACAGTTGGTAGTATTTTAAGGGGTTA ATTTACTCTGATTGGTGAAACC

615	<i>rocS_100down</i>	Cloning at <i>rocS</i> locus	R	GAAACCGATATAAACCGCATCGGCA
616	<i>rocS_2700down</i>	Cloning at <i>rocS</i> locus	R	GTCACGTTATTAGGCTTGGCGTATTTTC
617	<i>rocS_3000down</i>	Cloning at <i>rocS</i> locus	R	GCTGTTTGTTCACCTTAGGCTCG
533	<i>vc1639_3000up</i>	Cloning at <i>dbfS</i> locus	F	GCTTAGTGATCGCAGAGCTTGC
534	<i>vc1639_3000down</i>	Cloning at <i>dbfS</i> locus	R	GTGCACTGCATTATTGACTCGCTTAGC
535	<i>vc1639_100up</i>	Cloning at <i>dbfS</i> locus	F	CAAGATTTTGACCGCGATTCCAATAC
536	<i>vc1639_100down</i>	Cloning at <i>dbfS</i> locus	R	GTAGAGTTTCCAAACCTATAGGAG
626	<i>vc1639_Real_B</i>	<i>dbfS</i> deletion	R	CAACTGAAAATCCGTTTTTGCACCGCATTTAATTGGCATGCA ACTGATACCCAAG
627	<i>vc1639_Real_C</i>	<i>dbfS</i> deletion	F	CTTGGGTATCAGTTGCATGCCAATTAATGCGGTGCAAAAAC GGATTTTCAGTTG
559	<i>vc1639_2700up</i>	Cloning at <i>dbfS</i> locus	F	CAATCGGTGGTGCACAACCTATCTGAG
560	<i>vc1639_2700down</i>	Cloning at <i>dbfS</i> locus	R	GTTAATGACTTGGAGCAGAATTAAGTTAGCCGC
527	<i>vc1638_3000up</i>	Cloning at <i>dbfR</i> locus	F	GTAGGTCTTCTCGCACTTGTGTTTTG
528	<i>vc1638_3000down</i>	Cloning at <i>dbfR</i> locus	R	GTCCATAACCTTAGCGGAACCTCATG
529	<i>vc1638_100up</i>	Cloning at <i>dbfR</i> locus	F	GACAATCAAGTCTTTCGTGTCGAATACAAC
530	<i>vc1638_100down</i>	Cloning at <i>dbfR</i> locus	R	CTTCCAGCAAATATTGATGGATGAGATTTGGG
628	<i>vc1638_Real_B</i>	<i>dbfR</i> deletion	R	GAGATTTAATTGGCATGCAACTGATACCCAAGGTCTGCTCG ATTATTTTTTGTATGGCAGC
629	<i>vc1638_Real_C</i>	<i>dbfR</i> deletion	F	CGTGCCATCAAAAATAATCGAGCAGACCTTGGGTATCAGTT GCATGCCAATTAATCTC
557	<i>vc1638_2700up</i>	Cloning at <i>dbfR</i> locus	F	CACCATCCGTTTTGTGCATCATGATG
558	<i>vc1638_2700down</i>	Cloning at <i>dbfR</i> locus	R	GTGGCGTCAGATCCCAAACTTGTTTC
650	<i>dbfR_D51V_B</i>	Generating <i>dbfR<sup>D51V</sup></i>	R	CAATTCGGTAGGCCGAGTACGAGTACGATGACGTCC
651	<i>dbfR_D51V_C</i>	Generating <i>dbfR<sup>D51V</sup></i>	F	GGACGTCATCGTACTCGTACTCGGCCTACCGAAATTG
736	<i>dbfR_SNAP_delta_S_Gblock</i>	Gblock for generating <i>dbfR-SNAP</i> and simultaneously deleting <i>dbfS</i>	F	CGCGGTCTTGGGTATCAGTTGCATGCCAATTCAGGAAGCGG CTCAGGCAGCGGATCAGGAATGGATAAGGATTGTGAAATGA AGAGAACAACCTTAGATTCCCCACTAGGTAATTAGAATTAT CCGTTGCGAACAGGATTACATCGTATTATTTTTAGGAA AAGGAACCAAGTGCAGCAGACGCCGTAGAAGTACCAGCCCC CGCCGAGTTTTAGGAGGACCAGAACCCTAATGCAAGCCA CCGCTTGGTTAAACGCATATTTTCATCAACCAGAAGCCATAG AAGAATCCCAGTACCAGCCCTACACCACCCAGTATTTCAAC AAGAATCATTTACGAGACAAGTATTATGGAAATTATTAAGT CGTCAAATTCGGAGAAGTTATCAGCTATAGTCACCTAGCCG CTCTTGCCGGTAATCCAGCAGCCACTGCCGCAGTTAAACC GCATTATCAGGTAACCCAGTTCCCATATTAATTCATGCCAT AGAGTAGTACAAGGAGATTAGACGTCGGCGGATATGAAGG AGGTTTAGCAGTTAAAGAATGGTTACTAGCACATGAAGGACA TAGATTAGGTAACCAGGATTAGGTTAAATGCGGTGCAAAAAC CGGATTTTCAGTTGC
734	<i>dbfR_R</i>	Generating <i>dbfR-SNAP</i> and deleting <i>dbfS</i>	R	TTGGCATGCAACTGATACCCAAGACCGCG
735	<i>dbfS_down_F</i>	Generating <i>dbfR-SNAP</i> and deleting <i>dbfS</i>	F	ATGCGGTGCAAAAACCGGATTTTCAGTTGC
672	<i>SNAP_UnivR</i>	Generating <i>dbfR-SNAP</i>	R	TTAACCTAATCCTGGTTTACCTAATCTATGTCCTTCATGTGCT AGTAACC

718	<i>dbfR</i> _SNAP_E	Generating <i>dbfR</i> -SNAP	F	GACATAGATTAGGTAACCAGGATTAGGTTAAGATGTGATCA AAACTGTGCGCGGTC
634	<i>cdgl</i> _3000up	Cloning at <i>cdgl</i> locus	F	CGATGCAAGTAGCTGAACAAGCAC
635	<i>cdgl</i> _2700up	Cloning at <i>cdgl</i> locus	F	GAATACATTGACGCCGAGCGCTTTG
636	<i>cdgl</i> _100up	Cloning at <i>cdgl</i> locus	F	GGGAGCAACTTCACTGTATTCAATGAGTG
637	<i>cdgl</i> _B	<i>cdgl</i> deletion	R	GATGCGATCATCATGAGCTACCTATTTTTGTAAAGGCCCGAC TTCATTTTTTCTACTCTC
638	<i>cdgl</i> _C	<i>cdgl</i> deletion	F	GAGAGTAGAAAAAATGAAGTCGGCCTTTACAAAAATAGG TAGCTCATGATGATCGCATC
639	<i>cdgl</i> _100down	Cloning at <i>cdgl</i> locus	R	GGTCAGCAGCTTTTGCAGCACTTTATTG
640	<i>cdgl</i> _2700down	Cloning at <i>cdgl</i> locus	R	GAGGTGCAACCTGCGTGAAGTGGATTTTC
641	<i>cdgl</i> _3000down	Cloning at <i>cdgl</i> locus	R	CCAGTGAGGCTATCAATATGCGCATC
642	<i>cdgG</i> _3000up	Cloning at <i>cdgG</i> locus	F	GTGTCGATTCCAGCGACAAGTGCCAATTTG
643	<i>cdgG</i> _2700up	Cloning at <i>cdgG</i> locus	F	GAATACACCGCAGAGCCGATAGTGAC
644	<i>cdgG</i> _100up	Cloning at <i>cdgG</i> locus	F	GATAAATGCTGCCAGTCGGCATAAACACTGAG
645	<i>cdgG</i> _B	<i>cdgG</i> deletion	R	GCACAAATTAATAGTTAATTAGCTTAAATATTAATCAGACTGG ATAGTTGAGGATCAATCCTGATCC
646	<i>cdgG</i> _C	<i>cdgG</i> deletion	F	GGATCAGGATTGATCCTCAACTATCCAGTCTGATTAATATTT AAGCTAATTAATAATTTGTGC
647	<i>cdgG</i> _100down	Cloning at <i>cdgG</i> locus	R	TTGAGGCCATGCTAGAGCATGATGTTGAGC
648	<i>cdgG</i> _2700down	Cloning at <i>cdgG</i> locus	R	CCAGTAAATTCGGTTATGAGGTAAAGGATG
649	<i>cdgG</i> _3000down	Cloning at <i>cdgG</i> locus	R	GATCGCCACTTTCCGCGATTGGATG
105	BBC1881	Cloning at <i>vc1807</i> locus	F	TTTAAAGGGGATCAGTGACCG
106	BBC1882	Cloning at <i>vc1807</i> locus	R	CAATTTTGCTTTTGACCATCCC
270	<i>1807</i> _2700up	Cloning at <i>vc1807</i> locus	F	GGCCGGCACTTTGATTACAATC
271	<i>1807</i> _2700down	Cloning at <i>vc1807</i> locus	R	GTCTATATCAGAGCGCTTAAAGAGCG
721	<i>P<sub>BAD</sub></i> _1807_Univ_B	Generating <i>P<sub>BAD</sub></i> - <i>dbfS</i>	R	CATTTACACCTCCTGCAGGTAC
722	<i>P<sub>BAD</sub></i> - <i>dbfS</i> -1807_C	Generating <i>P<sub>BAD</sub></i> - <i>dbfS</i>	F	GTACCTGCAGGAGGTGTGAAATGGGTATCAGTTGCATGCCA ATTAATCTCG
723	<i>P<sub>BAD</sub></i> - <i>dbfS</i> -1807_D	Generating <i>P<sub>BAD</sub></i> - <i>dbfS</i>	R	GTCGACGGATCCCCGGAATTTAATGGATTTGACGGCTTTG GCTG
232	ABD123	Generating <i>P<sub>BAD</sub></i> - <i>dbfS</i>	F	ATTCCGGGGATCCGTGAC
729	<i>P<sub>BAD</sub></i> - <i>lapG</i> -1807_C	Generating <i>P<sub>BAD</sub></i> - <i>lapG</i>	R	GTACCTGCAGGAGGTGTGAAATGAAACGTTGGATTGTGCTG TCTCTGG
730	<i>P<sub>BAD</sub></i> - <i>lapG</i> -1807_D	Generating <i>P<sub>BAD</sub></i> - <i>lapG</i>	F	GTCGACGGATCCCCGGAATCTACTCATCATAGCTAAC TAGA GG
731	<i>P<sub>BAD</sub></i> - <i>rbmB</i> -1807_C	Generating <i>P<sub>BAD</sub></i> - <i>rbmB</i>	R	GTACCTGCAGGAGGTGTGAAATGCTGTTATACTTAAATCAAT TCAATAAAGAGGGTGG
732	<i>P<sub>BAD</sub></i> - <i>rbmB</i> -1807_D	Generating <i>P<sub>BAD</sub></i> - <i>rbmB</i>	F	GTCGACGGATCCCCGGAATTCATCTTTAATAAAGTGCTGTA TATAAATGGTCCG
724	<i>P<sub>BAD</sub></i> - <i>cheY3</i> -1807_Gblock	Generating <i>P<sub>BAD</sub></i> - <i>cheY3</i>	F	GTACCTGCAGGAGGTGTGAAATGGAGGCAATTTTGAATAAA AACATGAAGATCCTTATTGTTGATGACTTTTCAACAATGCGC CGAATCGTTAAAAACCTACTTCGAGATCTGGGGTTCAATAAC ACGCAGGAAGCGGACGATGGCCTAACGGCATTGCCTATGC TCAAGAAAGGTGATTTTACTTTGTAGTCACAGACTGGAATA TGCCCGGTATGCAAGGTATTGACTTGCTTAAAAATATCCGTG CCGACGAAGAACTGAAGCACCTGCCTGCTACTAATGATCACA



				GCAGAAGCCAAACGTGAGCAAATCATCGAAGCCGCTCAAGC AGGCGTGAATGGTTACATCGTAAAACATTACCGCTGCTAC GCTTAAAGAAAAATTAGACAAAATTTTGAGCGTTTATAAATT CCGGGGATCCGTCGAC
587	<i>tagA_3000up</i>	Cloning at <i>tagA</i> locus	F	GGGCTGCAAGAAGCTGGATCTGCTAC
588	<i>tagA_2700up</i>	Cloning at <i>tagA</i> locus	F	GAGCAAATTACAAGCTCGATCTTCAGCTAAG
662	<i>tagA_103bpD_B</i>	Removes first 103 codons of <i>tagA</i> including start	R	GTCAAATACTGGTCGTTACTGGATGTTGCATTCTTTAACAAA AAAATAAAGACAAGGGAAACGTATTG
663	<i>tagA_103bpD_C</i>	Removes first 103 codons of <i>tagA</i> including start	F	CAATACGTTTCCCTTGTCTTTATTTTTTTGTTAAAGAATGCAA CATCCAGTAACGACCAGTATTTGAC
591	<i>tagA_2700down</i>	Cloning at <i>tagA</i> locus	R	CCACCGAGGATACCATCCATCTTGATAATATG
592	<i>tagA_3000down</i>	Cloning at <i>tagA</i> locus	R	CTCTTGCCATCCATATGACATGATGTCTTTTG
593	<i>tagA_100up</i>	Cloning at <i>tagA</i> locus	F	GTGTGGCTTCATCCATTGACCTCCAATG
594	<i>tagA_100down</i>	Cloning at <i>tagA</i> locus	R	CCACTGCGAAATTAATTTTAGGATCAGCTTTAGC
664	<i>tagA_150down</i>	Cloning at <i>tagA</i> locus	R	GCAACCATACATCTTCCATTACTACCATAAGAG
519	Arbitrary Primer	Transposon localization	F	GGCCACGCGTCGACTAGTACNNNNNNNNNNAGAG
520	<i>Tn5</i> specific Primer	Transposon localization	R	GAAGCCCTTAGAGCCTCTC
521	Arbitrary PCR cleanup	Transposon localization	F	AGGAACACTTAACGGCTGAC
522	Arbitrary PCR cleanup	Transposon localization	R	GGCCACGCGTCGACTAGTAC

## References

1. C. Matz, *et al.*, Biofilm formation and phenotypic variation enhance predation-driven persistence of *Vibrio cholerae*. *Proc. Natl. Acad. Sci. U.S.A.* **102**, 16819–16824 (2005).
2. J. Yan, B. L. Bassler, Surviving as a community: Antibiotic tolerance and persistence in bacterial biofilms. *Cell Host Microbe* **26**, 15–21 (2019).
3. T. Shaw, M. Winston, C. J. Rupp, I. Klapper, P. Stoodley, Commonality of elastic relaxation times in biofilms. *Phys. Rev. Lett.* **93**, 098102 (2004).
4. J. Walter, R. A. Britton, S. Roos, Host-microbial symbiosis in the vertebrate gastrointestinal tract and the *Lactobacillus reuteri* paradigm. *Proc. Natl. Acad. Sci. U.S.A.* **108**, 4645–4652 (2011).
5. E. Roilides, M. Simitopoulou, A. Katragkou, T. J. Walsh, How biofilms evade host defenses. *Microbiology Spectrum* **3** (2015).
6. T. F. Mah, G. A. O'Toole, Mechanisms of biofilm resistance to antimicrobial agents. *Trends Microbiol.* **9**, 34–39 (2001).
7. P. L. Phillips, G. S. Schultz, Molecular mechanisms of biofilm infection: biofilm virulence factors. *Adv Wound Care (New Rochelle)* **1**, 109–114 (2012).
8. C. Guilhen, C. Forestier, D. Balestrino, Biofilm dispersal: multiple elaborate strategies for dissemination of bacteria with unique properties. *Mol. Microbiol.* **105**, 188–210 (2017).
9. L. Hobley, C. Harkins, C. E. MacPhee, N. R. Stanley-Wall, Giving structure to the biofilm matrix: an overview of individual strategies and emerging common themes. *FEMS Microbiol Rev* **39**, 649–669 (2015).
10. J. G. Conner, J. K. Teschler, C. J. Jones, F. H. Yildiz, Staying alive: *Vibrio cholerae*'s cycle of environmental survival, transmission, and dissemination. *Microbiol Spectr* **4** (2016).
11. S. Almagro-Moreno, K. Pruss, R. K. Taylor, Intestinal colonization dynamics of *vibrio cholerae*. *PLOS Pathogens* **11**, e1004787 (2015).
12. A. J. Silva, J. A. Benitez, *Vibrio cholerae* biofilms and cholera pathogenesis. *PLOS Neglected Tropical Diseases* **10**, e0004330 (2016).
13. A. L. Gallego-Hernandez, *et al.*, Upregulation of virulence genes promotes *Vibrio cholerae* biofilm hyperinfectivity. *Proc. Natl. Acad. Sci. U.S.A.* **117**, 11010–11017 (2020).
14. R. Tamayo, B. Patimalla, A. Camilli, Growth in a biofilm induces a hyperinfectious phenotype in *Vibrio cholerae*. *Infection and Immunity* **78**, 3560–3569 (2010).
15. M. Valentini, A. Filloux, Biofilms and cyclic di-GMP (c-di-GMP) signaling: Lessons from *Pseudomonas aeruginosa* and other bacteria. *J Biol Chem* **291**, 12547–12555 (2016).
16. J. G. Conner, D. Zamorano-Sánchez, J. H. Park, H. Sondermann, F. H. Yildiz, The ins and outs of cyclic di-GMP signaling in *Vibrio cholerae*. *Curr Opin Microbiol* **36**, 20–29 (2017).
17. J. C. N. Fong, K. A. Syed, K. E. Klose, F. H. Yildiz, Role of *Vibrio* polysaccharide (vps) genes in VPS production, biofilm formation and *Vibrio cholerae* pathogenesis. *Microbiology (Reading, Engl.)* **156**, 2757–2769 (2010).
18. A. A. Bridges, B. L. Bassler, The intragenus and interspecies quorum-sensing autoinducers exert distinct control over *Vibrio cholerae* biofilm formation and dispersal. *PLoS Biol.* **17**, e3000429 (2019).
19. P. K. Singh, *et al.*, *Vibrio cholerae* combines individual and collective sensing to trigger biofilm dispersal. *Curr Biol* **27**, 3359–3366.e7 (2017).
20. D. S. Merrell, D. L. Hava, A. Camilli, Identification of novel factors involved in colonization and acid tolerance of *Vibrio cholerae*. *Molecular Microbiology* **43**, 1471–1491 (2002).
21. R. Gao, A. M. Stock, Biological insights from structures of two-component proteins. *Annu Rev Microbiol* **63**, 133–154 (2009).
22. R. Gao, S. Bouillet, A. M. Stock, Structural basis of response regulator function. *Annu. Rev. Microbiol.* **73**, 175–197 (2019).

23. C. D. Boyd, D. Chatterjee, H. Sondermann, G. A. O'Toole, LapG, required for modulating biofilm formation by *Pseudomonas fluorescens* Pf0-1, is a calcium-dependent protease. *Journal of Bacteriology* **194**, 4406–4414 (2012).
24. J. C. N. Fong, F. H. Yildiz, The *rbmBCDEF* gene cluster modulates development of rugose colony morphology and biofilm formation in *Vibrio cholerae*. *Journal of Bacteriology* **189**, 2319–2330 (2007).
25. G. Kitts, *et al.*, A conserved regulatory circuit controls large adhesins in *Vibrio cholerae*. *mBio* **10** (2019).
26. A. J. Collins, T. J. Smith, H. Sondermann, G. A. O'Toole, From Input to Output: The Lap/c-di-GMP biofilm regulatory circuit. *Annu. Rev. Microbiol.* (2020) <https://doi.org/10.1146/annurev-micro-011520-094214>.
27. V. Berk, *et al.*, Molecular architecture and assembly principles of *Vibrio cholerae* biofilms. *Science* **337**, 236–239 (2012).
28. A. Seper, *et al.*, Extracellular nucleases and extracellular DNA play important roles in *Vibrio cholerae* biofilm formation. *Mol Microbiol* **82**, 1015–1037 (2011).
29. A. Hyakutake, *et al.*, Only One of the five *cheY* homologs in *Vibrio cholerae* directly switches flagellar rotation. *J. of Bacteriology* **187**, 8403–8410 (2005).
30. S. M. Butler, A. Camilli, Going against the grain: chemotaxis and infection in *Vibrio cholerae*. *Nat Rev Microbiol* **3**, 611–620 (2005).
31. S. M. Butler, A. Camilli, Both chemotaxis and net motility greatly influence the infectivity of *Vibrio cholerae*. *Proc Natl Acad Sci U S A* **101**, 5018–5023 (2004).
32. K. Son, J. S. Guasto, R. Stocker, Bacteria can exploit a flagellar buckling instability to change direction. *Nature Physics* **9**, 494–498 (2013).
33. N. A. Licata, B. Mohari, C. Fuqua, S. Setayeshgar, Diffusion of bacterial cells in porous media. *Biophys J* **110**, 247–257 (2016).
34. A. S. Utada, *et al.*, *Vibrio cholerae* use pili and flagella synergistically to effect motility switching and conditional surface attachment. *Nature Communications* **5**, 4913 (2014).
35. D. C. Wu, *et al.*, Reciprocal c-di-GMP signaling: Incomplete flagellum biogenesis triggers c-di-GMP signaling pathways that promote biofilm formation. *PLOS Genetics* **16**, e1008703 (2020).
36. S. Kojima, K. Yamamoto, I. Kawagishi, M. Homma, The polar flagellar motor of *Vibrio cholerae* is driven by an Na<sup>+</sup> motive force. *J Bacteriol* **181**, 1927–1930 (1999).
37. A. B. Dalia, E. McDonough, A. Camilli, Multiplex genome editing by natural transformation. *Proc Natl Acad Sci U S A* **111**, 8937–8942 (2014).
38. M. B. Miller, K. Skorupski, D. H. Lenz, R. K. Taylor, B. L. Bassler, Parallel quorum sensing systems converge to regulate virulence in *Vibrio cholerae*. *Cell* **110**, 303–314 (2002).
39. J. T. Saavedra, J. A. Schwartzman, M. S. Gilmore, Mapping transposon insertions in bacterial genomes by arbitrarily primed PCR. *Current Protocols in Molecular Biology* **118**, 15.15.1-15.15.15 (2017).
40. J. Yan, *et al.*, Mechanical instability and interfacial energy drive biofilm morphogenesis. *eLife* **8**, e43920 (2019).
41. B. Qin, *et al.*, Cell position fates and collective fountain flow in bacterial biofilms revealed by light-sheet microscopy. *Science* (2020) <https://doi.org/10.1126/science.abb8501>.
42. E. A. Groisman, The pleiotropic two-component regulatory system PhoP-PhoQ. *Journal of Bacteriology* **183**, 1835–1842 (2001).
43. L. R. Prost, M. E. Daley, M. W. Bader, R. E. Klevit, S. I. Miller, The PhoQ histidine kinases of *Salmonella* and *Pseudomonas* spp. are structurally and functionally different: Evidence that pH and antimicrobial peptide sensing contribute to mammalian pathogenesis. *Mol Microbiol* **69**, 503–519 (2008).